Surfaces and Interfaces 31 (2022) 101970

Contents lists available at ScienceDirect

Surfaces and Interfaces

journal homepage: www.sciencedirect.com/journal/surfaces-and-interfaces

Reduction and removal of methylene blue from aqueous solutions via recyclable magnetic gold nanomaterials

Emmanuel Jabulani Lukhele [a], Joyce Tsepiso Khutlane [b], Nikoletta B. Báthori [a], Rehana Malgas-Enus [b,*]

[a] Department of Chemistry, Faculty of Applied Sciences, Cape Peninsula University of Technology, P.O. Box 652, Cape Town 8000, South Africa
[b] Department of Chemistry and Polymer Science, Stellenbosch University, Private Bag X1, Stellenbosch 7602, South Africa

ARTICLE INFO

Keywords:
magnetic nanoparticles
SPIONs
gold-coated magnetic particles
dye removal
phosphine-stabilised nanoparticles
recyclable dye removal adsorbents

ABSTRACT

Nano-sized iron oxide particles displaying superparamagnetism (SPIONs), were synthesised using the co-precipitation method. Gold-coated SPIONs stabilised by phosphine ligands (1,3,5-triaza-7-phosphaadamantane (PTA) or triphenylphosphine (PPh_3)), were immobilised on the surface of these SPIONs. A total of 19 nano-magnetic systems were synthesised, with varying Au loading, stabilisers and reducing agents employed. The obtained nanomaterials were fully characterised by ultraviolet visible spectroscopy (UV–Vis), Fourier-transform infrared spectroscopy (FT-IR), powder X-Ray diffraction (PXRD), high-resolution transmission electron microscopy (HRTEM) and inductively coupled plasma spectroscopy (ICP). The PTA ligand was a better stabiliser than the PPh_3 ligand, resulting in more monodisperse nanoparticles for the former. These nanomaterials were subsequently used for the treatment of wastewater from the textile industry, specifically methylene blue (MB) reduction. The kinetics of this reaction using our range of nanomaterials are discussed. It was found that the adsorbents not only reduce the MB, but also remove it completely from the aqueous solution when extracting the nanomaterial by applying an external magnetic field. The MB was desorbed from the nanoparticle surface by acetonitrile, after which the adsorbent could easily be recycled up to 5 times. This reaction was also possible without using $NaBH_4$ as a reducing agent, albeit to a slower extent. The PTA-stabilized nanomaterials prepared with $NaBH_4$ as opposed to sodium citrate, proved to be the best adsorbent for the removal of MB from aqueous solution.

1. Introduction

The textile industry uses organic dyes, which leads to environmental pollution and contamination that is highly toxic to both flora and fauna. Industrial wastewater effluents contain toxic organic dyes such as azo dyes that affect the aquatic ecosystem. These toxic dyes can be removed from contaminated wastewater using various methods. [1] Conventional methods for removal of dyes from wastewater includes coagulation-flocculation, sedimentation, membrane technology, cloud point extraction, microbiological decomposition and chemical oxidation. However, these systems are not efficiently removing dyes from wastewater, hence as a result, the derivatives of the complex dyes remain in the water even after the treatment. [2,3] Therefore, the need to produce a safer and cleaner environment is of great importance. [4]

Methylene blue (MB) is a thiazine cationic dye which is predominately used in industry for dyeing cottons, colouring paper, wool and as temporary hair colorants. The increase in the use of MB dye is a major health hazard, as it is known to cause eye burns, which can result in blindness in humans. [5] The removal of azo dyes in wastewater treatment, using nanoparticles, is fast becoming the preferred technique for wastewater treatment. This removal technique has advantages such as high efficiency, being good adsorbates and ease of upscaling. The adsorption technique has received tremendous attention due to its cost efficiency, easy access with high performance, and of most importance, its reusability.

Nanoparticles possess remarkable catalytic, optical, magnetic, electronic, and thermal properties due to their small size, shape, and distribution as compared to their bulk analogues. [6] Nano-catalysts can be recovered and isolated by different methods such as centrifugation and filtration. The disadvantage of these methods is that they can hamper the sustainability and affordability of the nano-catalytic strategy. Making use of magnetic nanoparticles (MNPs) has become the most common

* Corresponding author.
E-mail address: rehana@sun.ac.za (R. Malgas-Enus).

https://doi.org/10.1016/j.surfin.2022.101970
Received 25 January 2022; Received in revised form 11 March 2022; Accepted 9 April 2022
Available online 19 April 2022

practical and logical solution as they can be removed from reaction mixtures using an externally applied magnetic field. Therefore, the MNPs have emerged to be ideal catalysts or supports for nano-catalyst systems going forward. This field of research has produced a great number of excellent reviews. [7]

The most promising particles are the iron oxide nanoparticles of various kinds, including their derivatives such as magnetite (Fe_3O_4), maghemite (γ-Fe_2O_3) and haematite (α-Fe_2O_3). Magnetite is the most commonly used magnetic material due to its ability to support important homogeneous catalytically active metals. [8] Surface functionalisation of superparamagnetic nanoparticles is a well-designed way to bridge the gap between heterogeneous and homogeneous catalysis. Gold nanoparticles are particularly promising materials for use as catalysts, due to their simple reductive preparation, reliable chemical stability especially when a ligand is used as a stabiliser (such as the phosphine ligands used in this research) and versatility in surface modification. [9] From the literature, it has been shown that gold nanoparticles are very efficient catalysts, especially for the reduction of 4-nitrophenol. Likewise, AuNPs have been used to catalyse reductive dye degradation for a few azo dyes. It is known that agglomeration is a huge challenge in nanoparticle synthesis since highly reactive small gold nanoparticles usually tend to agglomerate. Therefore, they also require stabilisers (such as phosphine ligands used, i.e., PTA and PPh_3) to ensure that agglomeration is limited and/or prevented. Both support materials and stabilising ligands can be modified successfully to prevent agglomeration for various applications. [10] Hence, researchers have focused on developing more effective methods for the treatment of wastewater. [11]

Here, we report the use of modified gold-coated magnetic nanoparticles stabilised with phosphine ligands as catalysts in the reduction and subsequent extraction of methylene blue in textile industry wastewater. These catalysts are also recyclable due to their magnetic properties. The effect of metal loading, ligand employed and reducing agent used is also discussed.

2. Experimental

2.1. Materials

Chemicals used include Methylene Blue ($C_{16}H_{18}ClN_3S\bullet 2H_2O$, molecular weight 355.90 g/mol, not less than 96%, $C_{16}H_{18}ClN_3S$ on dried, May & Baker Ltd); sodium borohydride granular (99.99% trace metal bass, Sigma-Aldrich); iron (III) chloride hexahydrate ($FeCl_3\bullet 6H_2O$, ACS reagent, 97%, Sigma-Aldrich); iron (II) sulphate heptahydrate ($FeSO_4\bullet 7H_2O$, ACS reagent, ≥99.0%, Sigma-Aldrich); triphenylphosphine (PPh_3, ReagentPlus®, 99%, Merck); ammonium hydroxide (NH_4OH, 28–30%, Sigma-Aldrich); absolute ethanol (CH_3CH_2OH, 99.8%, Merck); gold (III) chloride trihydrate ($HAuCl_4\bullet 3H_2O$, ≥49.0, Sigma-Aldrich); sodium citrate tribasic dihydrate ($Na_3C_6H_5O_7$, ≥99.0%, Sigma-Aldrich) and ultraspec solution gold (Au, 1000 ± 3 μg/ml, 20 ℃ Au metal 99.999% pure in 10% HNO_3); De Bryn spectroscopic solution iron (Fe, 1000 ± 3 μg/ml, 20 ℃, Fe metal 99.999% pure in 5% HNO_3) and type II water (deionized).

2.2. Instruments

The Fourier-transform infrared (FT-IR) spectra were recorded using a PerkinElmer spectrum two IR spectrometer. A very small amount of the sample was mixed with dried KBr salt, ground into a fine powder using the mortar and pestle and then pressed into a KBr-pellet. A pure KBr-pellet was used to obtain a background reference. The spectra were collected between 4000 and 400 cm^{-1}. All the FT-IR spectra were presented without background correction. The structural properties of the samples were analysed using powder X-ray diffraction. Measurements were performed using a multipurpose X-ray diffractometer D8-Advance from Bruker, operated in a continuous scan in locked coupled mode with Cu-K_α radiation. The sample is mounted in the centre of the sample holder on a glass slide and levelled up to the correct height. A position sensitive detector, Lyn-Eye, is used to record diffraction data at a typical speed of 0.5 s/step which is equivalent to an effective time of 92 s/step for a scintillation counter. A Shimadzu UV-1800 UV–Vis spectrophotometer with a CPS that has a temperature control unit was used. Quartz cuvettes were used for spectrum and kinetic analysis, respectively. Branson Model B200 Ultrasonic Cleaner, 120 V, operates on 110–120 V AC, 50–60 Hz, includes 5-minute timer, a wide variety of other applications include: instrument and clock parts, small geological samples, metal and plastic machine parts, small electrical and electronic components, used for sonification of the nanoparticles which was used for the reduction of methylene blue studies. High-resolution transmission electron microscopic (HRTEM) analysis was performed using a FEI Tecnai G2 Field Emission Gun (FEG) TEM, with a 2.5 Å point-to-point resolution, and operating at 200 kV. The samples were prepared by dropwise addition of the solution onto a copper grid. The sample was dried under a UV lamp and attached to the sample holder. The average particle size of the NPs were determined by counting about 200 – 250 particles by making use of the "ImageJ" public software. [12] Relative metal concentrations of the NPs were measured by Spectro Arcos Inductively coupled plasma-optical emission spectrometer (ICP-OES) instrument which was used to determine the gold concentration and loading on the magnetite surface. The Ametek, Spectro Arcos, ICP-OES spectrometer was used. The concentration of metal ions in the supernatant solutions was determined by Inductively Coupled Plasma Optical Emission Spectroscopy (ICP-OES) with a Liberty Series II spectrometer (Varian, Australia). The calibration standards were matrix complemented to acid concentrations of the samples.

2.3. Synthesis of naked superparamagnetic iron oxide nanoparticles (SPIONs)

The synthesis of the naked SPIONs (**EJL1**) was carried out using the reported chemical co-precipitation method. [13,14] The solution of the metal ion precursors were prepared by dissolving $FeCl_3\bullet 6H_2O$ (3.4 g, 0.0127 M) and $FeSO_4\bullet 7H_2O$ (4.2 g, 0.0275 M) in deionised water, in the molar ratio of 1:2 at a temperature of 23.5 ℃. An ammonium solution (NH_4OH, 28–30%, 12 mL) was added dropwise to the solution of the metal precursors, and the reaction mixture was vigorously stirred for 20 mins. A black precipitate was formed immediately, indicating the formation of the naked SPIONs (**EJL1**). The reaction was stirred further for 60 min to ensure complete reduction. The black solid was washed with deionised water by using the magnetic decantation method until the pH of the supernatant was 7.0. The final black solid was washed with ethanol (50 ml x 4). The SPIONs were dried in the oven at 60 ℃.

2.4. Synthesis of gold-coated SPIONs

The gold-coated SPIONs (**EJL2-EJL7**) with different gold loadings were prepared by adding a known amount of naked SPION (**EJL1**) (1 mM) and the appropriate amount of $HAuCl_4$ salt (100–600 mM) into a round bottom flask which was dissolved in degassed deionised water (20 mL) and stirred vigorously for 3 h. Then, a known amount of reducing agent, either being sodium borohydride ($NaBH_4$, 2.3×10^{-3} M) or sodium citrate ($Na_3C_6H_5O_7$, 2.0×10^{-4} M), was added to the round bottom flask and further stirred for 2 h to ensure the complete reduction of the gold onto the SPIONs surface. The precipitate was separated by magnetic decantation and washed with deionised water (5 ml). The final gold coated SPIONs were placed in the oven to dry at 60 ℃. The percentage yields achieved ranged from 70 – 98%.

2.5. Stabilisation of gold-coated SPIONs

The method used for the preparation of the stabilised gold-coated SPIONs involves taking a known amount (3 mM) of the gold-coated SPIONs (2.4) and placing it into a round bottom flask. A phosphine

Table 1
The nanomaterials sample codes and descriptions.

Catalysts	Ratio of naked SPIONs: Au	Reducing agent	Stabiliser ligands
EJL1	Magnetite (SPION)		
EJL2	1:0.1 (10:1)	$NaBH_4$	
EJL3	1:0.05 (50:1)	$NaBH_4$	
EJL4	1:0.01 (100:1)	$NaBH_4$	
EJL5	1:0.1 (10:1)	$Na_3C_6H_5O_7$	
EJL6	1:0.05 (50:1)	$Na_3C_6H_5O_7$	
EJL7	1:0.01 (100:1)	$Na_3C_6H_5O_7$	
EJL8	1:0.1 (10:1)	$NaBH_4$	PTA
EJL9	1:0.05 (50:1)	$NaBH_4$	PTA
EJL10	1:0.01 (100:1)	$NaBH_4$	PTA
EJL11	1:0.1 (10:1)	$Na_3C_6H_5O_7$	PTA
EJL12	1:0.05 (50:1)	$Na_3C_6H_5O_7$	PTA
EJL13	1:0.01 (100:1)	$Na_3C_6H_5O_7$	PTA
EJL14	1:0.1 (10:1)	$Na_3C_6H_5O_7$	PPh_3
EJL15	1:0.05 (50:1)	$Na_3C_6H_5O_7$	PPh_3
EJL16	1:0.01 (100:1)	$Na_3C_6H_5O_7$	PPh_3
EJL17	1:0.1 (10:1)	$NaBH_4$	PPh_3
EJL18	1:0.05 (50:1)	$NaBH_4$	PPh_3
EJL19	1:0.01 (100:1)	$NaBH_4$	PPh_3

ligand, either PTA (130 mM – 700 mM) or PPh_3 (80 mM – 400 mM), to match the metal loading ratio of a particular nanoparticles (**EJL8-EJL19**), was added to a round bottom flask and dissolved in a 50 mL of deionised water. These were stirred vigorously for 3 h. The solid product was separated by magnetic decantation and washed with deionised water (5 ml). The final phosphine-stabilised gold-coated SPIONs were placed in the oven to dry at 60 ℃. The resultant SPIONs were stored in a desiccator under an inert environment (nitrogen gas), sealed well with parafilm to ensure that they do not get exposed to air as they can easily oxidise.

2.6. Catalytic reduction of methylene blue

The methylene blue (2000 μL; 0.040 mM), water (800 μL), catalyst (326 – 353 μL, 1–2 mol% gold relative to substrate as indicated) were added to the cuvette to make a total volume of 3000 μL. The cuvette was then placed in the UV–Vis spectrophotometer with the cell holder temperature set at 25 ℃ (unless specified otherwise). The $NaBH_4$ (100 μL; 0.050 mM) was added, and the mixture was stirred quickly. The UV–Vis spectroscopy absorbence was recorded in the range of 900 – 190 nm or at the λ_{max} for the dye at 15 second intervals. The strong absorption bands of MB located at $\lambda = 666$ nm was closely monitored. For all UV–Vis spectroscopy data sets, the raw data were exported to Excel and processed further. All experiments were performed in triplicate, and the results were averaged, unless otherwise specified.

3. Results and discussion

3.1. Nanoparticle material design, synthesis and characterisation

The co-precipitation method involved reaction of Fe^{2+}/Fe^{3+} at the ratio of 1:2 with a base such as ammonium hydroxide. During the reaction, the colour of the iron precursor solution changed from yellow to brown then black. [15] The black colour signifies the formation of the naked SPIONs. Naked SPIONs exhibit a hydrophilic character due to the presence of hydroxyl groups on their surface which results in hydrophilic interactions between the particles, causing their agglomeration. Therefore, it is crucial that SPIONs are prepared in the presence of a stabilising agent.

In this study, naked SPIONs were coated with gold and then stabilised with two phosphine ligands, PPh_3 and PTA. The coating process was exploded by varying the amount of gold salt during the synthesis and using two reducing agents: sodium borohydride and sodium citrate. For instance, the first set of 6 gold coated SPIONs were prepared by varying the ratio between the naked SPIONs and Au salt. The following ratios (naked SPIONs: Au salt) were used: 1:10 (1:0.1), with the higher content of Au; followed by 1:50 (1:0.05), with the lesser Au content; and lastly 1:100 (1:0.01) with the least content of Au. As shown in the Table 1, these gold-coated SPIONs were prepared using one of the two reducing agents: either being sodium borohydride ($NaBH_4$) for 3 catalysts (**EJL2-EJL4**) and sodium citrate ($Na_3C_6H_5O_7$) for the other 3 catalysts (**EJL5-EJL7**). These were referred to as unstabilised gold-coated SPIONs. The gold-coated SPIONs were then stabilised producing 6 gold-coated SPIONs with a phosphine ligand, 1,3,5-Triaza-7-phosphaadamantane (PTA), (**EJL8-EJL13**), while the other 6 catalysts were

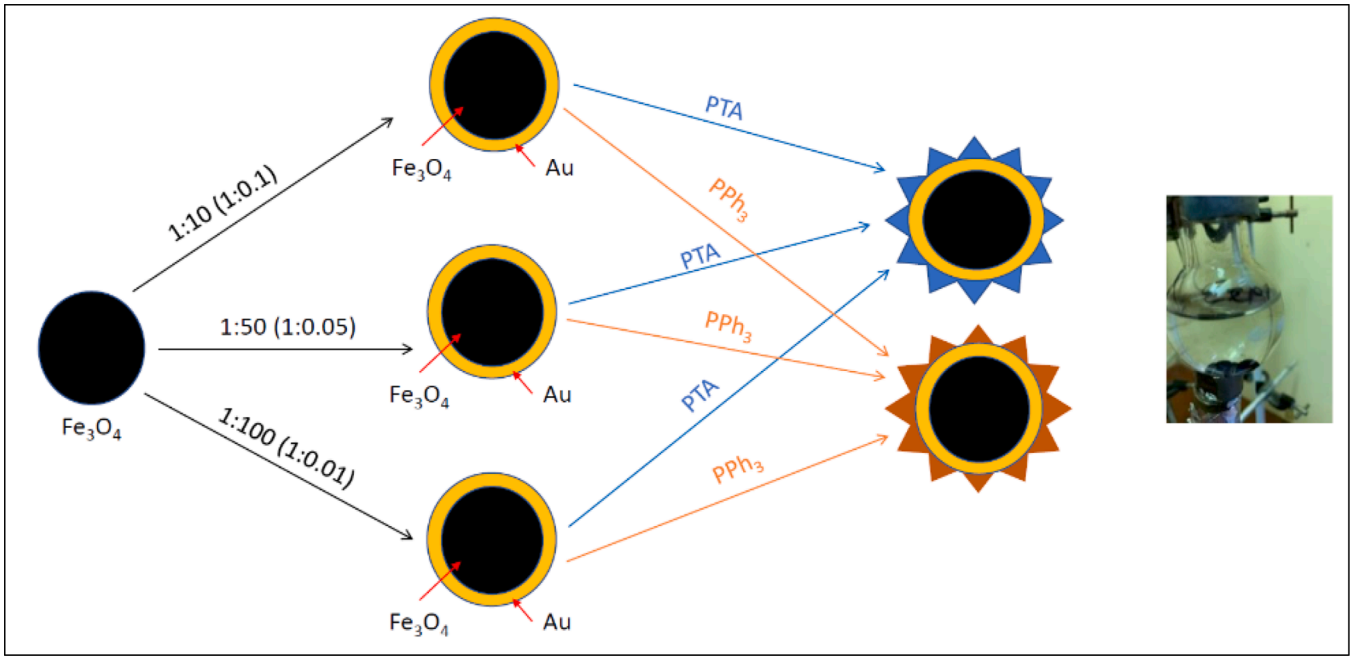

Fig. 1. Synthesis of ligand stabilised gold-coated SPIONs. (For interpretation of the references to colour in this figure legend, the reader is referred to the web version of this article.)

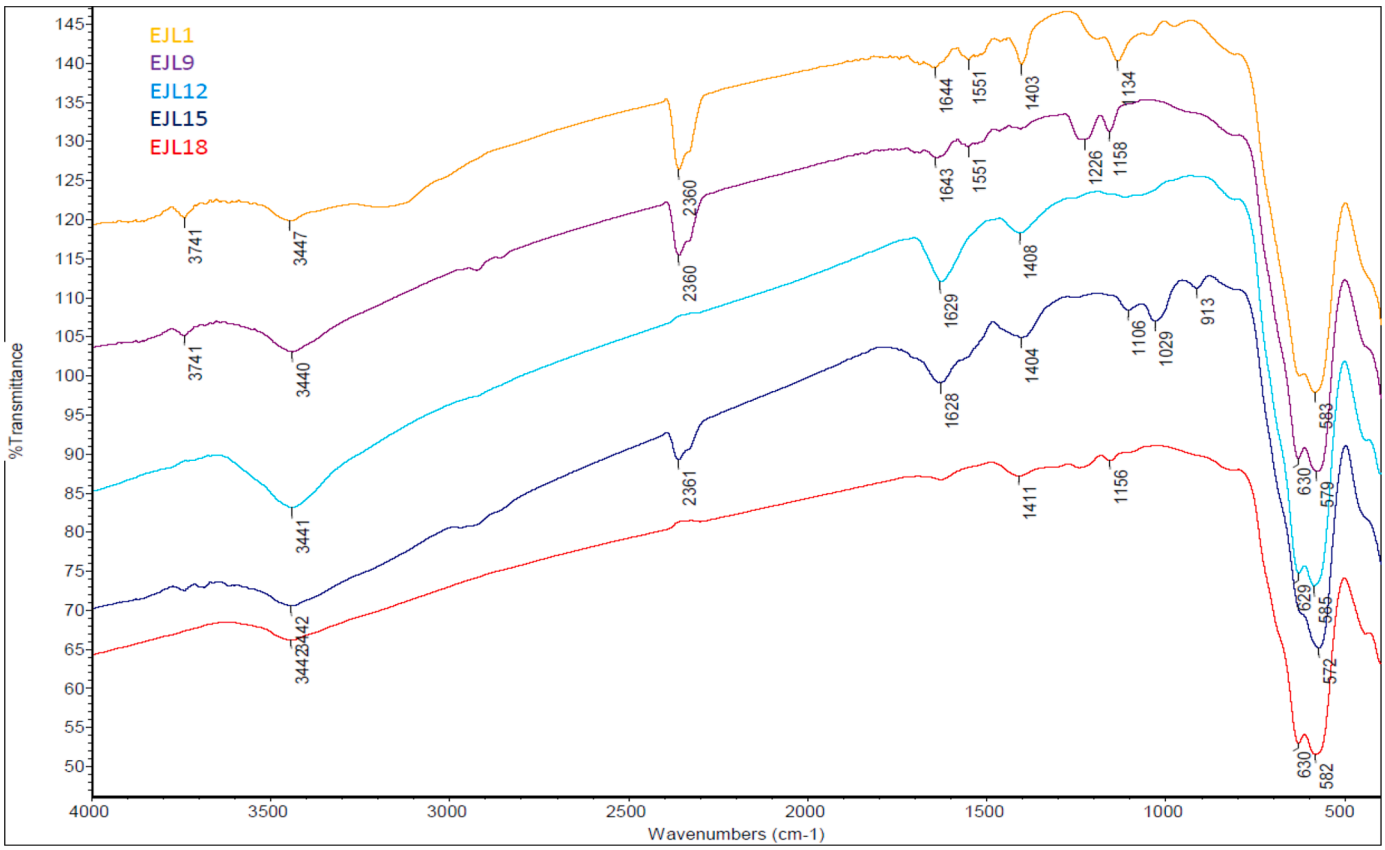

Fig. 2. Infra-red spectra of naked SPIONs and stabilised gold-coated SPIONs. (For interpretation of the references to colour in this figure legend, the reader is referred to the web version of this article.)

Table 2
List of IR absorption bands with peaks of interest.

Sample code	O-H ($cm^{(1)}$	FE—O ($cm^{(1)}$	C—N ($cm^{(1)}$	—CH ($cm^{(1)}$	Aryl C = C ($cm^{(1)}$	Aryl -CH OP* ($cm^{(1)}$
EJL1	3447	583				
EJL9	3440	579/ 630	1226/ 1158		1643	
EJL12	3441	585/ 629		1408	1629	
EJL15	3442	572	1106/ 1029	1404	1628	913
EJL18	3442	582/ 630	1156	1411	1628	

stabilised with a phosphine ligand, triphenylphosphine (PPh_3), (**EJL14-EJL19**). A total of 19 catalysts were synthesised for use in methylene blue reduction. Fig. 1 summarises the different ways in which the naked SPIONs were modified and stabilised, respectively. Also, refer to Fig. S1 and Fig. S2 in the ESI.

3.2. Characterisation of nanomaterials

The naked SPIONs as prepared was characterised using IR spectroscopy, as shown in Fig. 2. The naked SPIONs was diluted with KBr, grounded using a mortar and pestle, into fine powder, which was pressed into a KBr-pellet. Magnetite (naked SPIONs-**EJL1**) is a blended cubic oxide that contains $^{2}/_{3}$ Fe^{3+} and $^{1}/_{3}$ Fe^{2+} cations, respectively. Therefore, the absorption intensity at $\lambda = 583\ cm^{-1}$, can be assigned to Fe-O stretching vibration modes of the tetrahedral and octahedral sites, respectively. Moreover, the band's intensity at $\lambda = 2360\ cm^{-1}$ can be assigned to the stretching vibration of CO_2 in the atmosphere during analysis. The spectra also display additional intensity bands at around $\lambda = 1403\ cm^{-1}$ and $1134\ cm^{-1}$ and these bands can be attributed to the unreacted FeOOH or $Fe(OH)_2$ species, which is seen as the intermediates in the synthesis process of the formation of magnetite nanoparticles. The absorption peak at $3447\ cm^{-1}$ is observed and can be originated by the hydroxyl functionality (OH) present in water. The Fourier-transform infrared (FT-IR) spectra of unmodified as well as modified SPIONs were taken from the range 4000 – 400 cm^{-1}, in which the intensities of important bands were displayed. The vibrational frequency at 1627 cm^{-1} observed in the FT–IR spectra of sodium citrate treated gold-coated SPIONs (**EJL6**) is characteristic of the carboxylate functional group, whilst the medium intensity frequency at 1402 cm^{-1} represents the -CH vibration. These results confirmed the attachment of sodium citrate on the naked SPIONs surface.

In the IR spectra of stabilised gold-coated SPIONs (**EJL9-EJL19**), characteristic C = C vibrational stretches at around 1628 – 1643 cm^{-1} were observed. Whilst the medium intensity frequency at around 1404 – 1411 cm^{-1} represents the -CH vibration. These results confirmed the coordination of sodium citrate on the magnetite nanoparticles' surface. The IR spectrum of **EJL12** has a frequency at 913 cm^{-1} indicative of the aromatic -CH out-of-plane bending vibrations. There was also bending frequencies at around 1029 – 1226 cm^{-1}, which can be assigned to the C—N amine functionality in **EJL9, EJL15** and **EJL18.** These results confirmed the coordination of the two different phosphine ligands to the gold-coated magnetite nanoparticles. The metal ratio of the 1:50 samples was used for the FT-IR representative spectra. See also Table 2. for the monitored vibrational frequencies of interest in this study. Also, refer to Fig. S3 which compared naked SPIONs, unstabilised gold-coated SPIONs and stabilised gold-coated SPIONs in the ESI.

3.2.1. Powder X-Ray diffraction (PXRD) of the SPIONs

Powder Xray diffract (PXRD) was used to determine the crystallinity

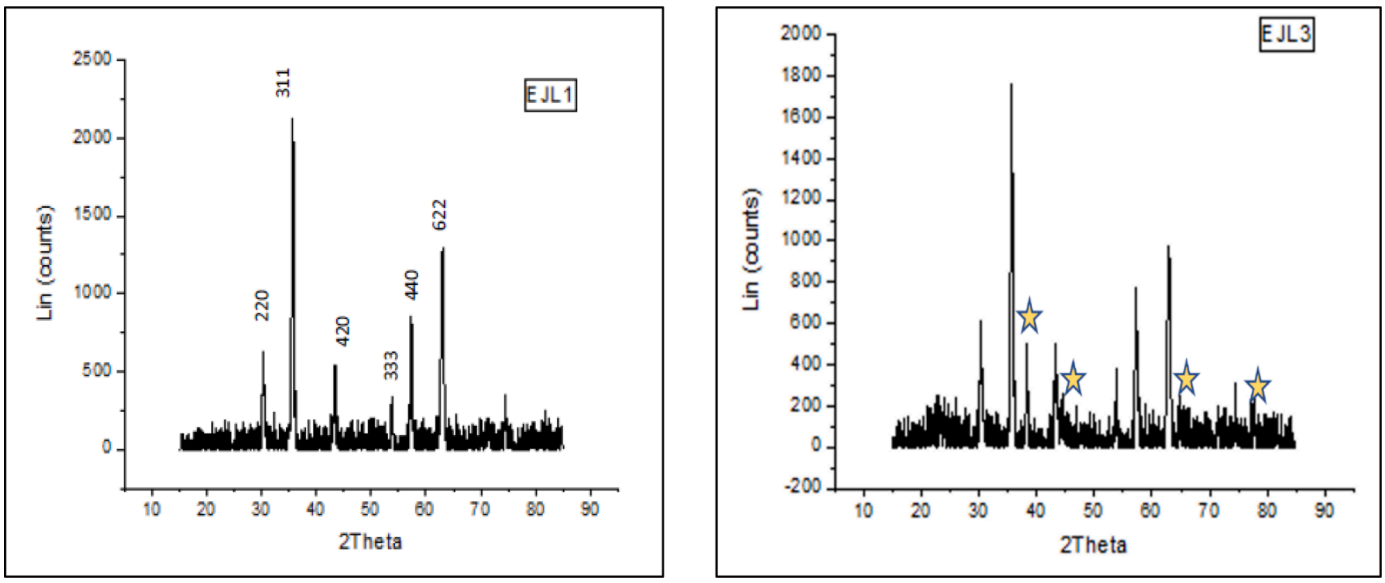

Fig. 3. Powder X-Ray Diffraction (PXRD) analysis of the naked SPIONs and gold-coated SPIONs. (For interpretation of the references to colour in this figure legend, the reader is referred to the web version of this article.)

and phase purity of the naked SPIONs unstabilised and stabilised gold coated SPIONs, respectively. Fig. 3 shows diffractograms of naked SPIONs, that exhibit Miller indices (*hkl*) values at 220, 311, 400, 422, 333, 440 and 622. This diffraction pattern match well with those specifically of standard magnetite samples, as per JCPDS cards No. 00–011–0614 with a cubic spine structure. In addition to these diffraction peaks, an additional peak associated with gold/syn peaks are shown as gold stars on the PXRD pattern. These were found for all the gold-coated and stabilised gold-coated SPIONs (**EJL2-EJL19**). The latter also exhibited diffraction patterns that matches with the standard magnetite as per as per JCPDS cards No. 00–011–0614 signifying that the modified SPIONs did not lose their crystallinity and structural properties. The strong and sharp peaks confirms that the gold coated SPIONs were crystalline. Also, the coating process did not result in the phase change of the SPIONs. [16]

3.2.2. *High-resolution transmission electron microscopy (HRTEM)*

The HRTEM analysis was conducted to determine the average particle size, size distribution, and morphology of naked SPIONs (**EJL1**). The three images taken at 50 nm, 20 nm and 10 nm images shows spherical agglomerated and polydisperse nanoparticles. The size distribution of particle dimension on average was found to be 18.7 ± 5.6 nm.

Furthermore, the HRTEM analysis was conducted to determine the average particle size, size distribution, and morphology of stabilised of unstabilised and stabilised gold coated SPIONs (**EJL2-EJL19**). Fig. 4 shows the TEM images and their corresponding particle size histograms of gold coated SPIONs (**EJL2** – **EJL11**). The TEM images for **EJL1, EJL12** – **EJL19** are shown in Figure S4 and Figure S5, respectively, in the ESI.

From the TEM images (Fig. 4), all the particles seem to be spherical, and some images show agglomerated and polydisperse nanoparticles. The average particle sizes in nm are listed in Table 3. The average particle sizes of gold-coated SPIONs that are stabilised with phosphine ligands, gave a particle size range of 17 – 20 nm. However, the gold-coated SPIONs that were not stabilised with phosphine ligands have a broader particle size range of 16 nm – 27 nm. This confirms that the ligands does stabilise the SPIONs and therefore prevent their agglomeration.

Table 3. The average particle sizes of gold coated SPIONs that are stabilised with phosphine ligands, gave a particle size range of 17 – 20 nm.

However, the gold coated SPIONs that were not stabilised with phosphine ligands have a broader particle size range of 16 nm – 27 nm. This confirms that the ligands do stabilise the SPIONs and therefore prevent their agglomeration.

3.2.3. *Ultraviolet visible spectroscopy (UV–Vis)*

This technique was used to confirm nanoparticle formation by detecting the surface plasmon resonance (SPR) band. The naked SPIONs as prepared were characterised using UV–Vis spectroscopy. The chromatogram of the naked SPIONs showed a very visible SPR peak at $\lambda =$ 390 nm which is characteristic of magnetite nanoparticles.[17] No other peaks were observed in the spectrum, indicating the high purity of the synthesised magnetite by the co-precipitation method. Fig. 5 represents UV-Vis absorption spectra of the naked SPIONs and gold-coated SPIONs. This gold-coated SPIONs were modified by reducing gold onto the surface of the naked SPIONs resulting in increased absorbence maxima corresponding to the SPR bands for the gold-coated SPIONs, compared to the naked SPIONs that only showed a singular visible SPR peak at $\lambda =$ 390 nm. The SPR peak for the gold-coated SPIONs prepared using $NaBH_4$ as a reducing agent showed absorbence peaks at $\lambda = 260$ nm and 380 nm, respectively. There are also two SPR peaks observed at $\lambda = 290$ and 350 nm for the gold-coated SPIONs prepared using $Na_3C_6H_5O_7$ as a reducing agent. These results indicate the successful reduction of the gold onto the SPIONs surface, resulting in gold-coated SPIONs.

3.2.4. *Inductively coupled plasma optical emission spectroscopy*

The ICP-OES results presented in a bar chart, Fig. 6, shows the metal loading for **EJL8-EJL19**. When comparing the metal loadings of the ratios for catalysts set group [**EJL8** (1:10), **EJL9** (1:50) and **EJL10** (1:100)], the Au content decreases from the highest Au content, 1:10 (1:0.1), to the lowest Au content, 1:100 (1:0.01), proving that the Au metal loading was performed successfully and was coated directly to the surface of the SPIONs. This trend was expected for these gold-coated SPIONs, as the highest Au content was in 1:10 ratio, followed by 1:50, with 1:100 having the least Au content used and is clearly observed in all four sets, as seen in Fig. 6.

3.3. *Effect of ligand on NPs shape and stability*

The stability of the 1,3,5-triaza-7-phosphaadamantane (PTA) and triphenylphosphine (PPh_3) stabilised gold-coated SPIONs was evaluated using **EJL10** and **EJL19**, respectively. Using TEM and UV–Vis

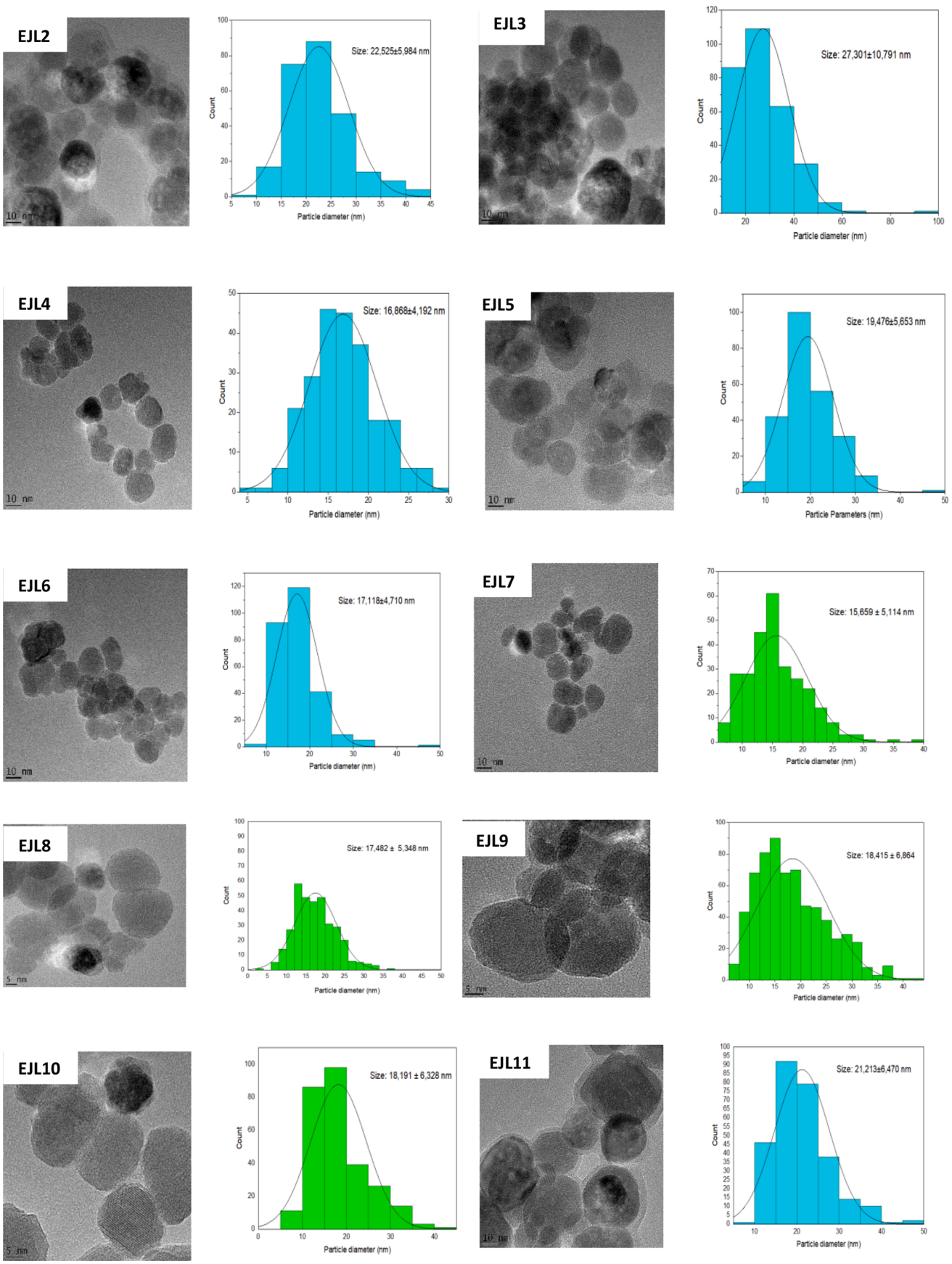

Fig. 4. HRTEM images, particle size histograms of the unmodified gold-coated SPIONs, PTA stabilised gold-coated SPIONs and PPh_3 stabilised gold-coated SPIONs (EJL2-EJL11). (For interpretation of the references to colour in this figure legend, the reader is referred to the web version of this article.)

Table 3
Summary of average particle sizes of the naked SPIONs, unstabilised and stabilised gold-coated SPIONs.

Sample codes	Ratio of Fe_3O_4: Au	Reducing agent	Stabiliser (ligands)	Average particle sizes (nm)
EJL2	1:0.1 (10:1)	$NaBH_4$		22.53 ± 6.0
EJL3	1:0.05 (50:1)	$NaBH_4$		18.73 ± 6.0
EJL4	1:0.01 (100:1)	$NaBH_4$		27.30 ± 10.8
EJL5	1:0.1 (10:1)	$Na_3C_6H_5O_7$		16.87 ± 4.2
EJL6	1:0.05 (50:1)	$Na_3C_6H_5O_7$		19.48 ± 5.7
EJL7	1:0.01 (100:1)	$Na_3C_6H_5O_7$		17.12 ± 4.7
EJL8	1:0.1 (10:1)	$NaBH_4$	PTA	17.48 ± 5.3
EJL9	1:0.05 (50:1)	$NaBH_4$	PTA	18.42 ± 6.9
EJL10	1:0.01 (100:1)	$NaBH_4$	PTA	18.19 ± 6.3
EJL11	1:0.1 (10:1)	$Na_3C_6H_5O_7$	PTA	21.21 ± 6.5
ELJ12	1:0.05 (50:1)	$Na_3C_6H_5O_7$	PTA	16.75 ± 5.4
EJL13	1:0.01 (100:1)	$Na_3C_6H_5O_7$	PTA	17.99 ± 5.4
EJL14	1:0.1 (10:1)	$Na_3C_6H_5O_7$	PPh_3	18.66 ± 5.1
EJL15	1:0.05 (50:1)	$Na_3C_6H_5O_7$	PPh_3	20.40 ± 6.2
EJL16	1:0.01 (100:1)	$Na_3C_6H_5O_7$	PPh_3	19.50 ± 5.5
EJL17	1:0.1 (10:1)	$NaBH_4$	PPh_3	17.38 ± 6.0
EJL18	1:0.05 (50:1)	$NaBH_4$	PPh_3	17.42 ± 4.7
EJL19	1:0.01 (100:1)	$NaBH_4$	PPh_3	17.92 ± 5.2

techniques, we could observe the difference in the phosphine ligands from the TEM images as well as the UV–Vis spectrum. Fig. 7 shows the TEM images of **EJL10** and **EJL19**, respectively. It is clear from comparing the TEM images, that the PTA ligand is a better stabilizer than the PPh_3 ligand. The TEM images of the PTA stabilised catalysts show much more spherical shapes, and the NPs are sitting on top of one another compared to the more agglomerated PPh_3 stabilised gold-coated SPIONs. It seems that the latter agglomerated because of a large free surface energy of each nanoparticle. The images of the PTA stabilised

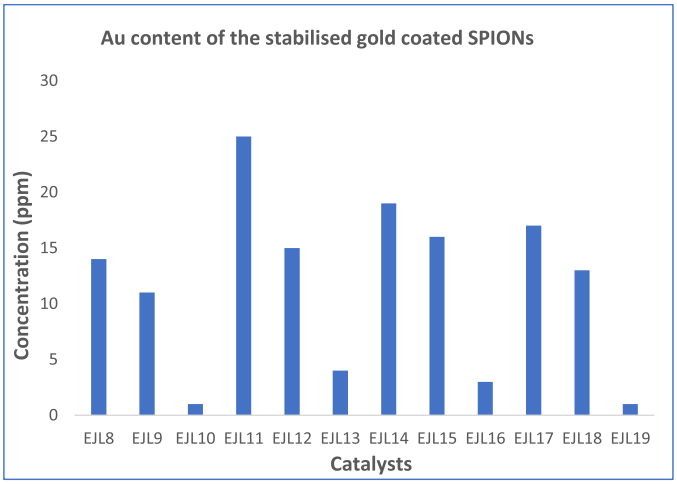

Fig. 6. ICP results for Au extractions of gold-coated SPIONs (**EJL8** to **EJL19**). (For interpretation of the references to colour in this figure legend, the reader is referred to the web version of this article.)

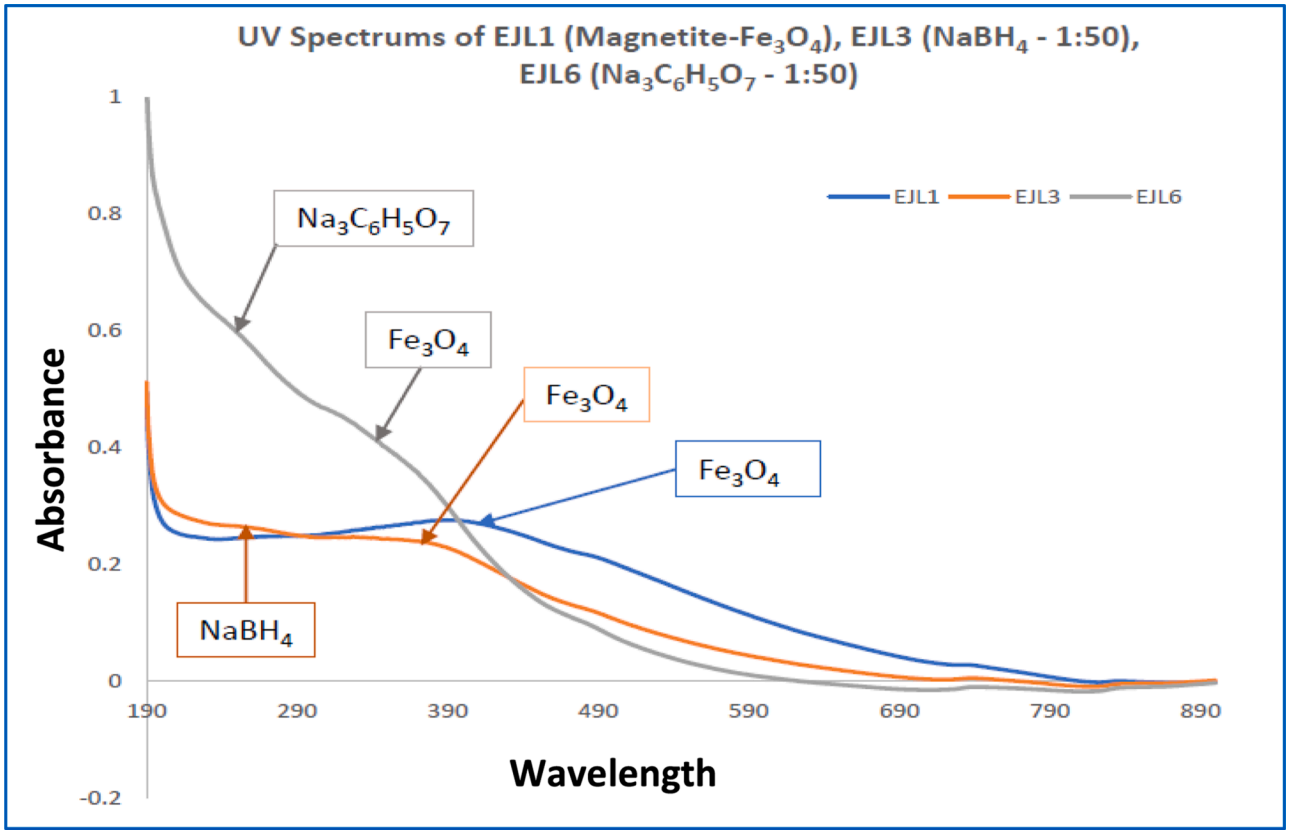

Fig. 5. UV–Vis spectra of the naked SPIONs (**EJL1**) and gold-coated SPIONs (**EJL3** and **EJL6**). (For interpretation of the references to colour in this figure legend, the reader is referred to the web version of this article.)

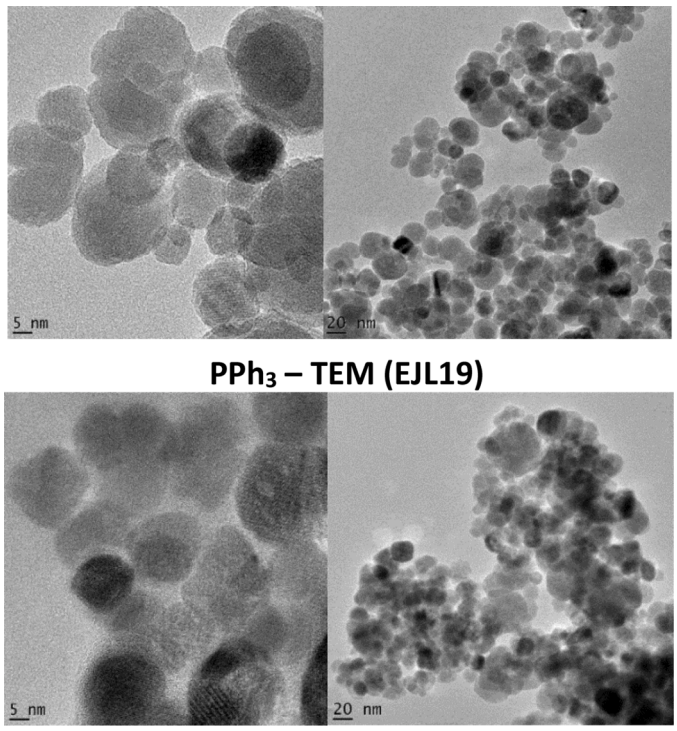

Fig. 7. Comparison of TEM images of PPh_3 stabilised gold-coated SPIONs vs PTA stabilised gold-coated SPIONs. (For interpretation of the references to colour in this figure legend, the reader is referred to the web version of this article.)

Table 4
TEM analysis for particle dimension size of gold-coated SPIONs prepared within a two-year period.

Sample code	2021 (nm)	2020 (nm)	Difference
EJL8 ($NaBH_4$ + PTA) 10:1	17,48 ± 5,3	16,94 ± 4,4	0,6 nm
EJL9 ($NaBH_4$ + PTA) 50:1	18,42 ± 6,9	16,11 ± 4,3	2,3 nm
EJL10 ($NaBH_4$ + PTA) 100:1	18,19 ± 6,3	16,41 ± 4,4	1,8 nm
EJL17 ($NaBH_4$ + PPh_3) 10:1	17,68 ± 6,0	16,39 ± 4,8	1,3 nm
EJL18 ($NaBH_4$ + PPh_3) 50:1	17,41 ± 4,7	17,92 ± 5,6	0,5 nm
EJL19 ($NaBH_4$ + PPh_3) 100:1	17,92 ± 5,2	20,47 ± 6,2	2,6 nm

particles are more well-defined, whilst the images of the PPh_3 stabilised particles are fuzzy. Also, the samples stabilised with PTA seems to be more monodisperse. Both stabilised ligands are more prone to form spherical shaped particles.

Fig. S6 (ESI) shows the UV–Vis spectra of the gold-coated SPIONs modified using PTA and PPh_3 ligands, respectively, where a similar sample reduced with sodium citrate and stabilised by PPh_3 versus PTA (**EJL9, EJL12** vs **EJL15, EJL18**) was investigated. It shows that the PTA stabilised gold-coated SPIONs have two bands, one at around 390 nm and another at around 750 nm, whilst PPh_3 stabilised gold-coated SPIONs shows one at about 280 nm and another at exactly 750 nm, as per the PTA spectrum. The band at 750 nm could be assigned to the effect of the reducing agent. The other SPR's at 390 nm and 280 nm show a slight shift from the SPIONs, which had an SPR at around 350 nm. The shift could be assigned to the effect of the ligands on the gold-coated SPIONs, and this confirms that the nanoparticles formed are slightly different due to the observed SPRs for the two phosphine ligands.

3.4. Reproducibility studies

The reproductivity studies for the synthesis of the PTA stabilised gold-coated SPIONs was studied using **EJL8** – **EJL10** samples while the PPh_3 stabilised gold-coated SPIONs were studied using **EJL17** – **EJL18** samples. The samples were prepared as previously described and the TEM analyses results are as shown in Table 4. The results show a slight difference in average particle sizes of the samples prepared in each respective year, signifying the stability of both PTA and PPh_3 gold-coated SPIONs. For instance, PPh_3 stabilised gold-coated SPIONs shows a very small difference in the average particle size with a range of 0.5 to 2.6 nm. It showed that a year later the synthesised gold-coated SPIONs gave similar results with the newly prepared ones. Based on TEM micrographs, it is also concluded that the phosphine stabilized gold-coated SPIONs prepared using the $NaBH_4$ or $Na_3C_6H_5O_7$ as reducing agent do not easily agglomerate. The UV–Vis spectra (Fig. S8 in the ESI) record in 2020 vs 2021 were similar, indicating that the structural properties of the SPIONs did not change. Hence, the UV–Vis results corroborate with the TEM results.

4. Reductive discoloration of methylene blue (MB)

Methylene blue (MB) ($C_{16}H_{18}ClN_3S$), which was used as an adsorbate in the present study, was prepared by dissolving the methylene blue (solid phase) in double-distilled water. The absorption spectra of the methylene blue are characterised by three main bands, one in the visible region (max = 666 nm), and two in the UV region (max = 293 nm and max = 260 nm). In our case, the most important band is at 666 nm as it clearly shows the decrease in absorbence with MB reduction. Methylene blue is blue in colour but turns colourless when forming Leuco-methylene blue (LMB), when it is exposed to a reducing agent [18]. The MB absorption band (650 – 670 nm) can be assigned to monomeric (MB^+) species. The UV–Vis spectra at 666 nm were monitored at different time intervals for MB dye reduction (see Fig. 8). As the monitored absorbence maxima intensity decreases, a slight shift in absorbance is noted. This is due to the addition of the PTA stabilised gold-coated SPIONs (**EJL8**) which helps in the electron relay from the BH_4^- (donor) to MB (acceptor).

4.1. The kinetic study for the reduction of MB

The reduction of MB by using $NaBH_4$ and the catalysts was a complicated process, probably due to various reduced forms of MB^+. The process could not easily be depicted by simple reaction kinetics. To estimate the kinetics rate of discoloration, an equation form of power law is used as shown in Eq. (1): [18]

$$-\frac{d[C]}{dt} = k[NaBH_4]^n[C]^m \quad (1)$$

Where k is the removal rate constant, [C] is MB concentration, m and n are the pseudo-order of reaction with respect to MB and Cat, respectively. The rate equation can be stated with an observed rate constant (K_{obs}) as follows, Eq. (2) and (3):

$$-\frac{d[C]}{dt} = kobs\ [C]^m \quad (2)$$

$$kobs = k\ [NaBH_4]^n \quad (3)$$

For a zero-order reaction and first-order reaction, the above equation after integration becomes Eq. (4) and (5):

$$Ct = kot \quad (4)$$

$$In(Ct) = In(Co) - k1t \quad (5)$$

In which C_0 is the initial MB concentration and C_t being the concentration at reaction time t.

The pseudo-first order kinetic plots (Fig. 9), using **EJL8** as a catalyst, shows a linear relationship with $R^2 \geq 0.97$ confirming that the MB reduction follows the pseudo-first order kinetics model. The reactions on

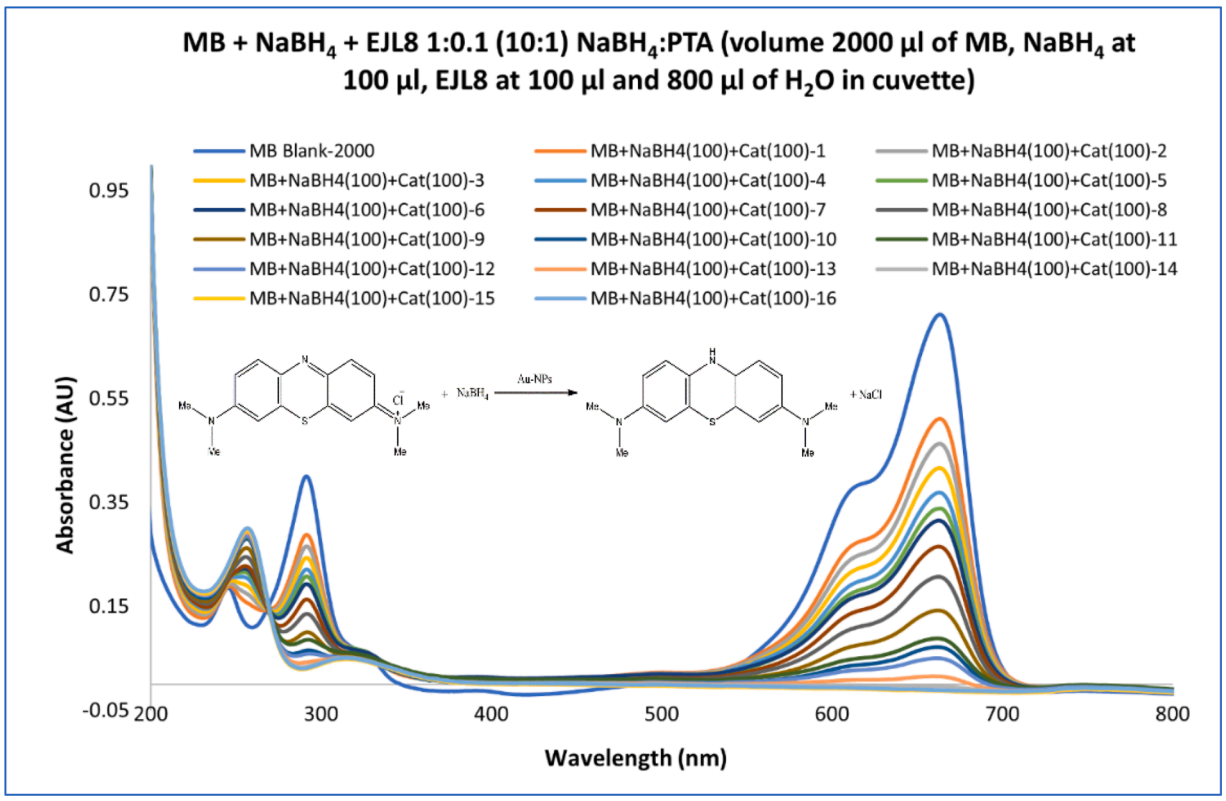

Fig. 8. Study of MB reduction, with EJL8 and $NaBH_4$ against time. Inset shows the schematic representation of the MB reduction with $NaBH_4$.

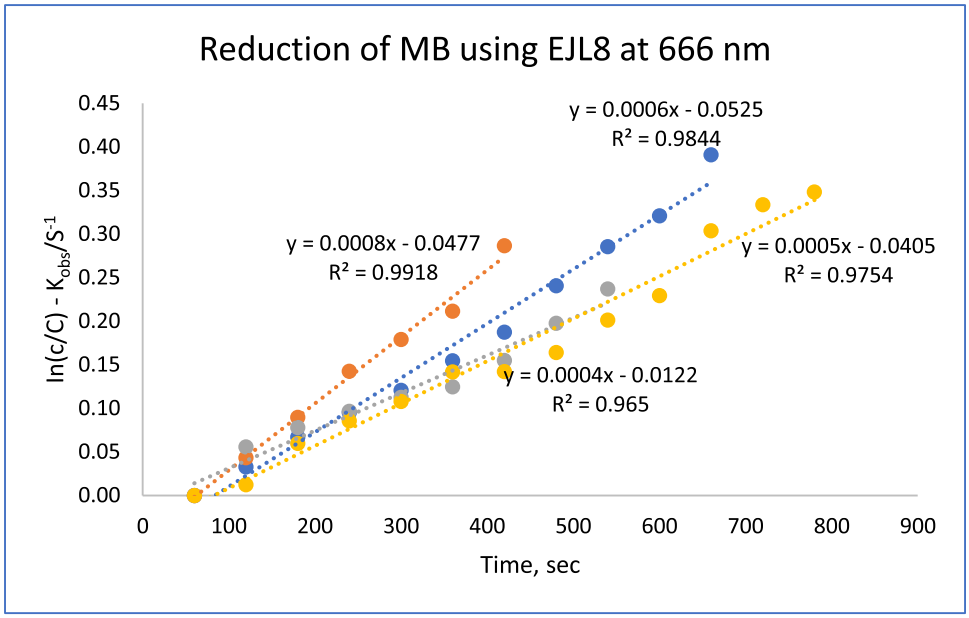

Fig. 9. The pseudo first order kinetic plot for MB reduction using EJL8 as ,catalyst at wavelengths λ = 666 nm.

the UV–Vis spectroscopy were run in quadruple. After the UV–Vis spectra were obtained, the K_{obs} were calculated for absorbence values at λ = 666 nm. The R^2 values were also taken into consideration.

4.2. Optimisation studies

The optimisation for the reduction of MB with $NaBH_4$ was performed using **EJL8** as a model catalyst. In addition, the reaction was optimised by varying the change in MB concentration (0.06 M – 0.24 M), $NaBH_4$ (0.000325 M – 0.0021 M) concentration, and change in catalyst loading (10 M – 100 M) while the other conditions remained the same (Table S1, in the ESI). The K_{obs} from the results produced the plots shown in Fig. 10. From these results it was evident that there is a correlation between the K_{obs} and the concentrations of the MB and $NaBH_4$, as well as the catalyst loading. For the concentration of MB, it was observed that as the MB concentration decreases, the rate constant increases.

This proved that when there is a lower MB concentration in the system, the reduction of MB occurs more rapidly. For the change in

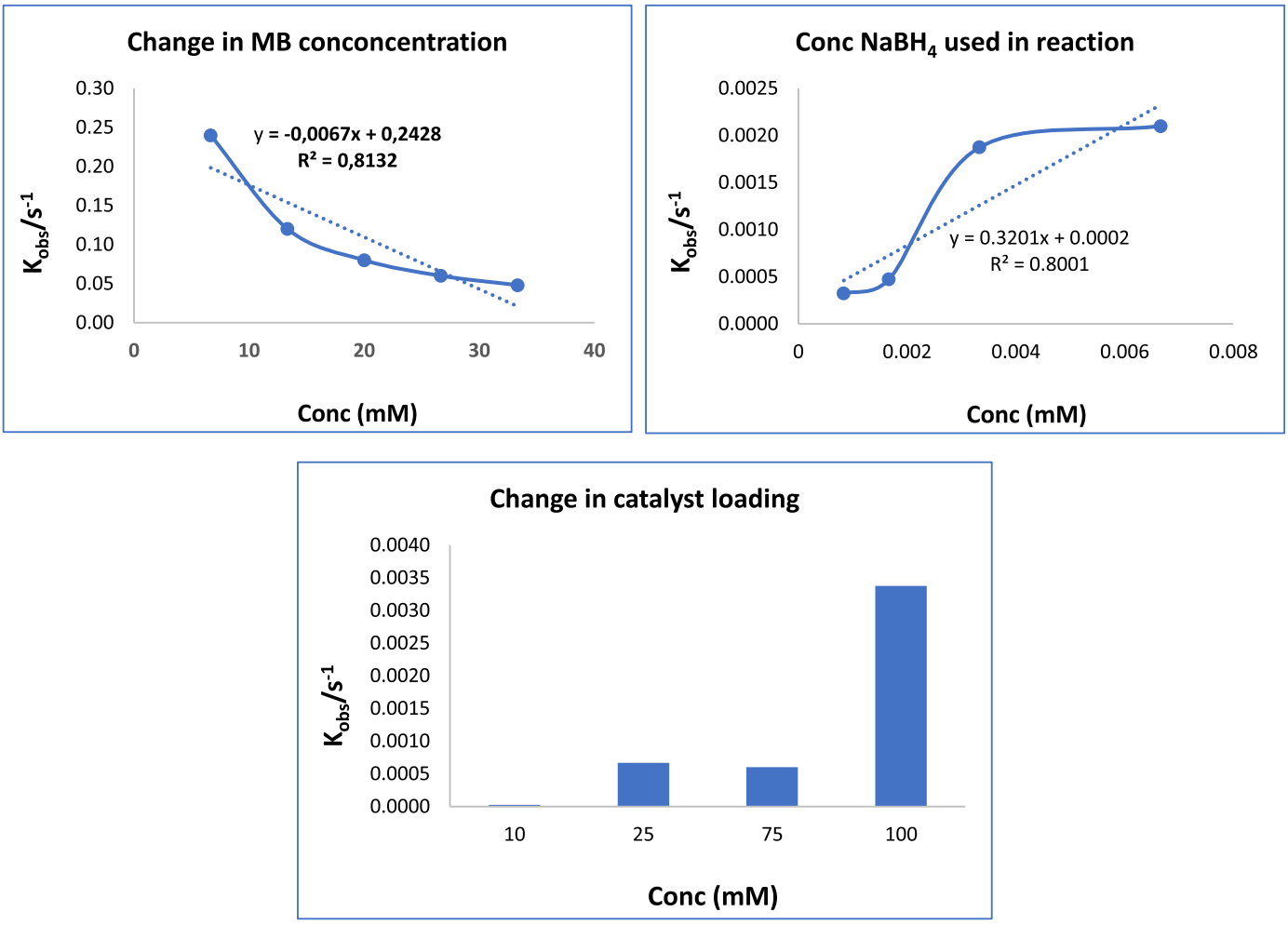

Fig. 10. The effect of MB concentration, $NaBH_4$ concentration and catalyst loading on catalytic reduction of MB.

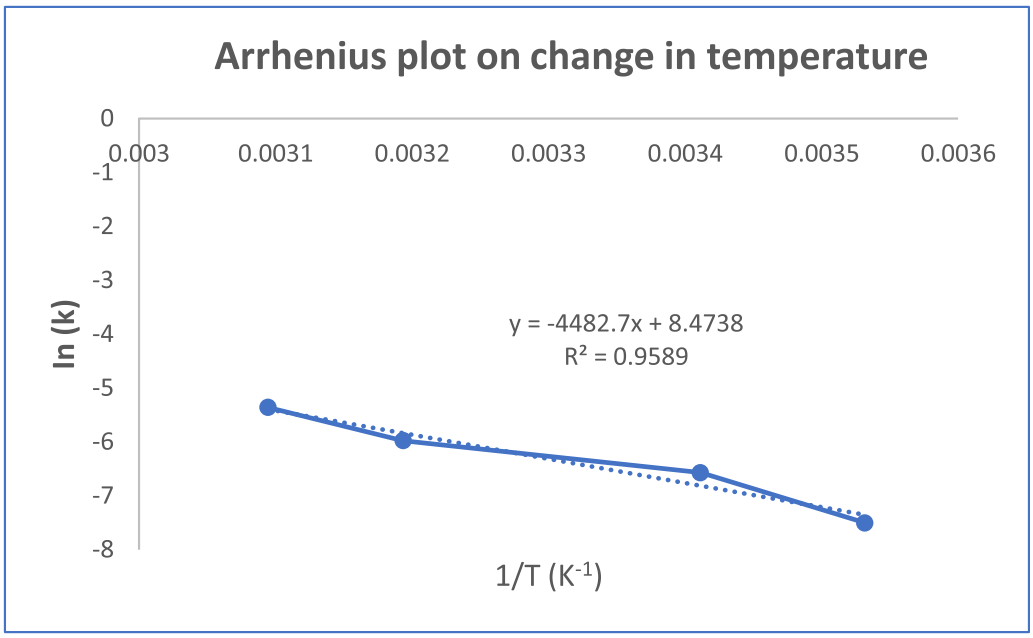

Fig. 11. Arrhenius plot for catalytic reduction of MB using EJL8 at constant concentrations but varying the temperature.

Table 5
Thermodynamic parameters for the reaction between MB and $NaBH_4$ in the presence of gold coated SPIONs.

Temperature (K)	K_{obs}	Activation energy (E_a) KJ/mol	$\Delta H^{\#}$KJ/mol	$\Delta S^{\#}$KJ/mol	$\Delta G\#$KJ/mol
283.15	0.00055	20.237	30.963	−0.1094	61.940
293.15	0.00140	18.444	29.872	−0.1019	59.744
313.15	0.00253	18.160	30.566	−0.0975	61.098
323.15	0.00470	17.080	29.924	−0.0926	59.848

$NaBH_4$ concentration, it was shown that a higher concentration of $NaBH_4$ resulted in a higher rate constant. This result correlates with findings of similar work in the literature. For instance, Meijboom et al. studied the reduction of 4-nitrophenol (4-NP) and observed the same trend for the effect of 4-NP and $NaBH_4$, respectively. [19] The catalyst loading concentration also showed a similar trend as for $NaBH_4$, in that a higher concentration results in an increased rate constant, as expected.

The effect of temperature on the reduction of methylene blue in the presence of a catalyst using UV-Vis spectroscopy was investigated in the range of 283 – 323 K (10 – 50 °C). To calculate the activation energies for the MB reduction, kinetics runs were carried out at various temperatures (283 K, 293 K, 313 K and 323 K). The results in Fig. 11 shows that the reduction efficiency has a direct proportionality to the reaction temperature. The increase in temperature may lead to an increasing reduction rate of methylene blue. This observation can be explained in terms of collision theory. [19]

The activation parameters associated with the reduction of MB are calculated from the plot of *In* K_{obs} versus $^1/_T$, which gives the value of activation energy (E_a), according to the Arrhenius equation:

$$In\ kobs = \frac{-Ea}{RT} + In\ A \tag{6}$$

In Eq. (6) the, the slope, $m = -\ \frac{Ea}{R}$

From Arrhenius plot in Fig. 11, the activation energy for the reduction of MB was calculated to be 20.237 KJ/mol at 283.15 K; 18.444 KJ/mol at 293.15 K; 18.160 KJ/mol at 313.15 K and 17.080 KJ/mol at 323.15 K (Table 4).

Using the Eq. (8)

$$k = Ae^{-Ea/RT} \tag{8}$$

where A is Arrhenius constant (2.71828), T is the temperature in Kelvin, and k is the rate constant, the Activation energy, E_a was obtained. The natural logarithm of the rate constant *In(k)* vs. the inversed temperature $^1/_T$, tells of the corresponding orders as zero ($M*s^{-1}$), one (s^{-1}) or two ($M^{-1}*s^{-1}$). For our purpose, corresponding order used was one (s^{-1}).

The value of $\Delta H^{\#}$ and $\Delta S^{\#}$ can be calculated from Eyring plot, Eq. (9):

$$In\left(\frac{kabs}{T}\right) = \left(In\frac{kB}{h} + \frac{\Delta S\#}{R}\right) - \frac{\Delta H\#}{RT} \tag{9}$$

Where, k_B is the Boltzmann's constant ($1.381\times10–23\ J.K^{-1}$); h is Plank's constant (6.626×10^{-34} J.s), and $In\frac{kB}{h} = 23.76$.

From the linear plot *of In* (K_{obs}/T) versus $^1/_T$, values of $\Delta H^{\#}$ and $\Delta S^{\#}$ can be calculated. The Gibbs' free energy $\Delta G^{\#}$ can therefore be calculated from the relation:

$$\Delta G^{\#} = \Delta H^{\#} - T\Delta S^{\#} \tag{10}$$

Table 5 shows the rate constants and activation energies in the range of temperature studied (283 – 323 K) with the thermodynamic

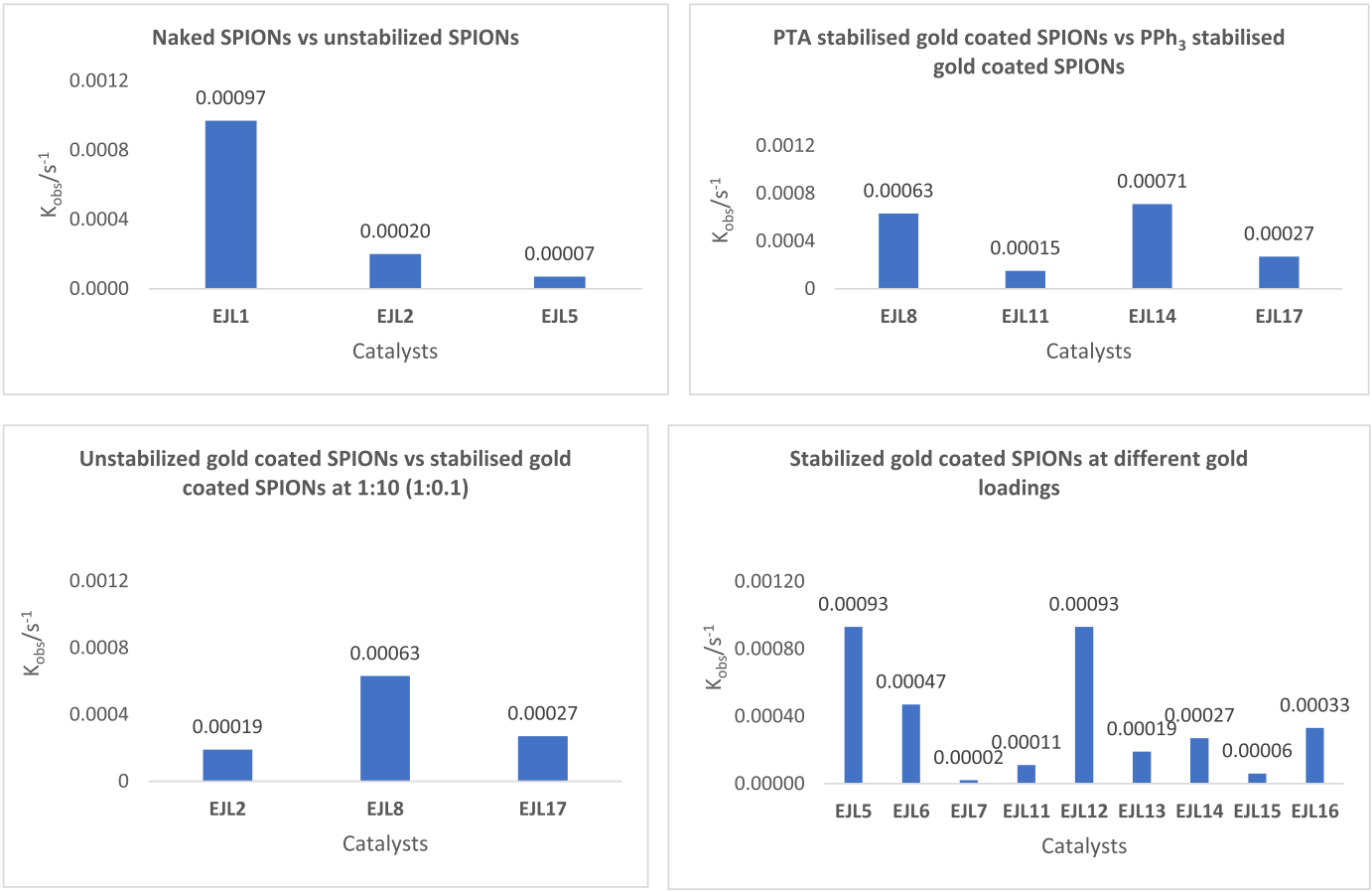

Fig. 12. Comparisons of the catalysts in MB reduction.

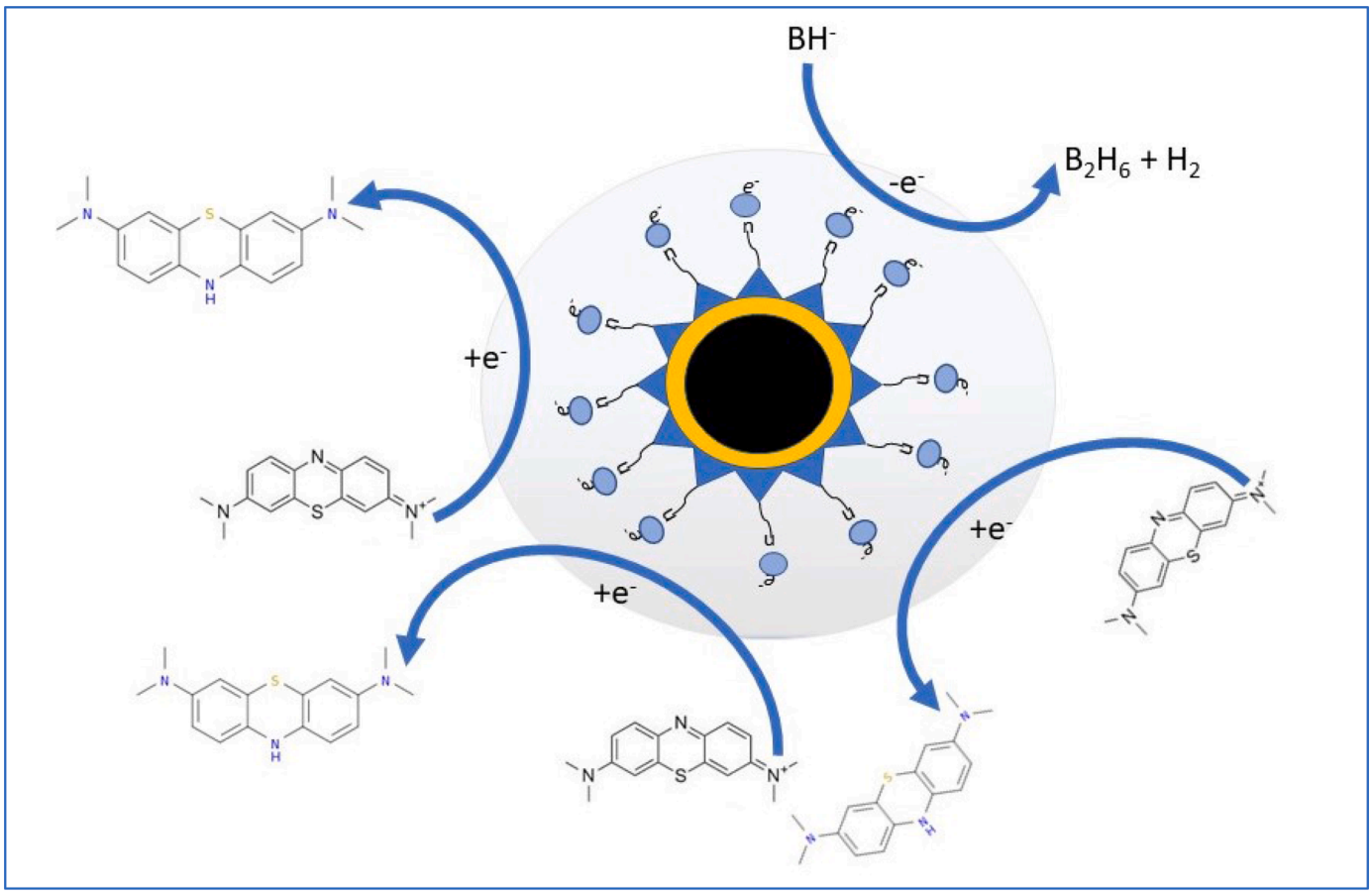

Fig. 13. Proposed electron transfer mechanism, where electrons from $NaBH_4$ are transferred to methylene blue via the catalyst's surface. (For interpretation of the references to colour in this figure legend, the reader is referred to the web version of this article.)

Table 6
The removal of MB dye in aqueous solution with SPIONs in the presence of the reducing agent ($NaBH_4$).

Catalyst Code	Ratio Fe_3O_4:Au	Reducing agent	Stabilizer	Catalysts (mg)	Order of MB removal
EJL9	1:0.05 (50:1)	$NaBH_4$	PTA	100.0	1
EJL3	1:0.05 (50:1)	$NaBH_4$		30.2	2
EJL15	1:0.05 (50:1)	$Na_3C_6H_5O_7$	PPh_3	29.7	3
EJL6	1:0.05 (50:1)	$Na_3C_6H_5O_7$		29.9	4
EJL12	1:0.05 (50:1)	$Na_3C_6H_5O_7$	PTA	30.0	5
EJL1	Magnetite			29.6	6

parameters of $\Delta H^{\#}$, $\Delta S^{\#}$ and $\Delta G^{\#}$. The positive values of $\Delta G^{\#}$ for the reaction (Table 5) indicate the non-spontaneous nature of decolonisation of MB by the AuNP catalyst at the temperatures studied. The negative value of $\Delta S^{\#}$ suggests the decrease in randomness at the liquid/liquid solution interface during the decolonisation of MB solution by gold-coated SPIONs, while the positive values of $\Delta H^{\#}$ show the endothermic nature of the reaction.

4.3. Comparisons of the catalysts in MB reduction

After the method optimisation studies were performed, each of the 19 catalysts, as synthesised, were used at the optimised reaction conditions. Based on the optimisation method, all the catalytic conditions for methylene blue reduction took place at 25 °C. The change in the absorbence of MB with time was monitored by UV–Vis spectroscopy at λ = 666. The reactions were run in quadruple for each catalyst using the reaction conditions: **methylene blue** – 2000 μL; **$NaBH_4$** - 100 μL; **catalyst** – 100 μL: **temp**. 25 °C, and the K_{obs} and R^2 were calculated at λ = 666 nm. The K_{obs} and R^2 evaluated at λ = 666 nm were used to have a better understanding of the different catalysts used for the reduction of MB and their possible mechanisms. To evaluate the catalyst efficacy for the reduction of MB, optimised reaction conditions were used to compare the K_{obs} determined using all the prepared catalysts.

4.3.1. Naked SPIONs vs unstabilised gold-coated SPIONs

By comparing the K_{obs} of naked SPIONs (**EJL1**) with the K_{obs} of 0.00097, to the unstabilised gold-coated SPIONs (**EJL2**) with the K_{obs} of 0.00020 and **EJL5** with the K_{obs} of 0.00007, it can be concluded that the naked SPIONs (**EJL1**) performed better than unstabilised gold-coated SPIONs (Fig. 12) when compared with the gold-coated SPIONs reduced using sodium borohydride (**EJL2**) versus sodium citrate (**EJL5**) reducing agent without any stabilising phosphine ligands. Even though the catalyst **EJL1** was better, it was unable to retain the reduction of MB as there was a reverse observation made of MB retaining a slight blue colour after 24 hrs of MB reduction. This was not observed with **EJL2** and **EJL5**; the solution of MB was clear.

4.3.2. PTA stabilised gold-coated SPIONs vs PPh_3 stabilised gold-coated SPIONs

The comparison between PTA stabilised gold-coated SPIONs (**EJL8**) with K_{obs} value of 0.00063 vs PPh_3 stabilised gold-coated SPIONs (**EJL17**) with K_{obs} value of 0.00027 shows that **EJL8** is favoured over

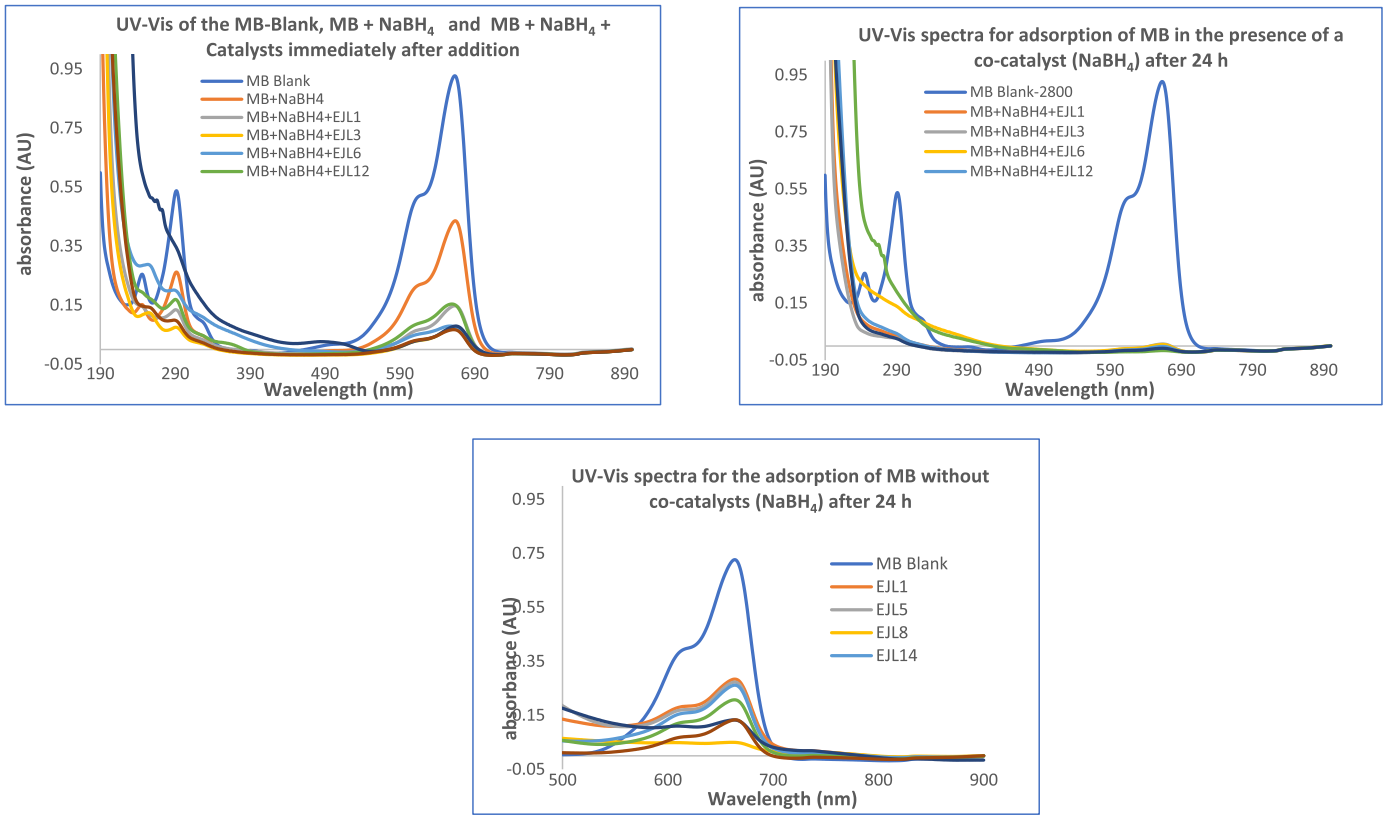

Fig. 14. The UV–Vis spectra of MB solution with co-catalysts ($NaBH_4$) and catalysts added. The UV–Vis spectra after 24 hrs once the catalysts were extracted from the MB aqueous solutions. The UV–Vis spectra of MB solution with nanomagnetic catalysts added at λ = 666 nm.

Table 7
The removal of MB dye in aqueous solution with SPIONs in the absence of the reducing ($NaBH_4$).

Catalyst Code	Ratio Fe_3O_4:Au	Reducing agent	Stabilizer	Catalysts (mg)	Order of MB removal
EJL8	1:0.01 (10:1)	$NaBH_4$	PTA	55.2	1
EJL17	1:0.01 (10:1)	$NaBH_4$	PPh_3	55.0	2
EJL2	1:0.01 (10:1)	$NaBH_4$		54.2	3
EJL11	1:0.01 (10:1)	$Na_3C_6H_5O_7$	PTA	54.8	4
EJL14	1:0.01 (10:1)	$Na_3C_6H_5O_7$	PPh_3	55.1	5
EJL5	1:0.01 (10:1)	$Na_3C_6H_5O_7$		54.5	6
EJL1	Magnetite			55.1	7

EJL17 as it has the higher k_{obs} value. It should be noted that both catalysts were prepared using $NaBH_4$ as a reducing agent. Furthermore, PTA stabilised gold-coated SPIONs (**EJL11**) with K_{obs} value of 0.00015 vs PPh_3 stabilised gold-coated SPIONs (**EJL14**) with K_{obs} value of 0.00071 showed that **EJL14** is favoured over **EJL11** as it has the higher k_{obs} value. The latter were prepared using $Na_3C_6H_5O_7$ as a reducing agent (Fig. 12). From these results, the reducing agent has an effect of the activity of the nanoparticle, depending on the ligand employed.

Comparing the stabilised gold-coated SPIONs using PPh_3, **EJL17** has a K_{obs} value of 0.00027, whilst **EJL14** has a K_{obs} value of 0.0007. When comparing the stabilised gold-coated SPIONs using PTA, **EJL8** has a K_{obs} value of 0.00063 whilst **EJL11** has a K_{obs} value of 0.00015. It can be concluded from comparing the two different reducing agents with the PPh_3 as a stabiliser that they react similarly in the MB reduction (**EJL17** vs **EJL14**) as shown in Fig. 12. It also can be concluded that the use of $NaBH_4$ as a reducing agent with PTA as ligand resulted in the best catalysts for MB reduction (**EJL8** vs **EJL11**), as it has the highest K_{obs} value.

4.3.3. *Unstabilised gold-coated SPIONs vs stabilised gold-coated SPIONs*

To determine the effect of NP stabilisation, unstabilised gold-coated SPIONs (**EJL2**), was compared to PTA stabilised gold-coated SPIONs (**EJL8**) and PPh_3 stabilised gold-coated SPIONs (**EJL17**) at the metal loading ratio of 1:0.1 (1:10). **EJL2** has a K_{obs} value of 0.00019, **EJL8** has a K_{obs} of 0.00063 and **EJL17** has a K_{obs} value of 0.00027. For the metal loading of 1:0.05 (1:50), **EJL3** has a K_{obs} value of 0.00012, **EJL9** has a K_{obs} of 0.00017 and **EJL18** has a K_{obs} value of 0.00033. For the metal loading of 1:100, **EJL4** has a K_{obs} value of 0.00029, **EJL10** has a K_{obs} of 0.00027 and **EJL19** has a K_{obs} value of 0.00027. From Fig. 12, it can be concluded that at metal loading ratio 1:0.1 (1:10), the PTA ligand stabilised catalyst was preferential for the MB reduction (**EJL2** vs **EJL8** vs **EJL17**) as it has the higher K_{obs} value. For the metal loading ratio 1:0.05 (1:50), it can be concluded that the PPh_3 stabilised catalyst was preferential for the MB reduction (**EJL3** vs **EJL9** vs **EJL18**) shown in Figure S9 in the ESI, as it has the highest K_{obs} values.

4.3.4. *Stabilized gold-coated SPIONs at different gold loadings*

To compare the stabilised gold-coated SPIONs at different gold to naked SPION ratios (1:10; 1:50 and 1:100), the catalysts prepared using $Na_3C_6H_5O_7$ as a reducing agent and stabilized by PTA were used. The K_{obs} were plotted as shown in Fig. 12. **EJL11** has a K_{obs} value of 0.00015, **EJL12** has a K_{obs} value of 0.00057 and **EJL13** has a K_{obs} value of 0.00025. From Fig. 12, it can be concluded that the favourable naked SPIONs:Au ratio for MB reduction is the 1:50 (1:0.05) compared to the 1:10 (1:0.01) and 1:100 (1:0.01), as it has the highest K_{obs} value (**EJL11** vs **EJL12** vs **EJL13**). For the $Na_3C_6H_5O_7$ analogues, at a metal loading ratio of 1:10, **EJL5** has a K_{obs} value of 0.00093, **EJL11** has a K_{obs} of

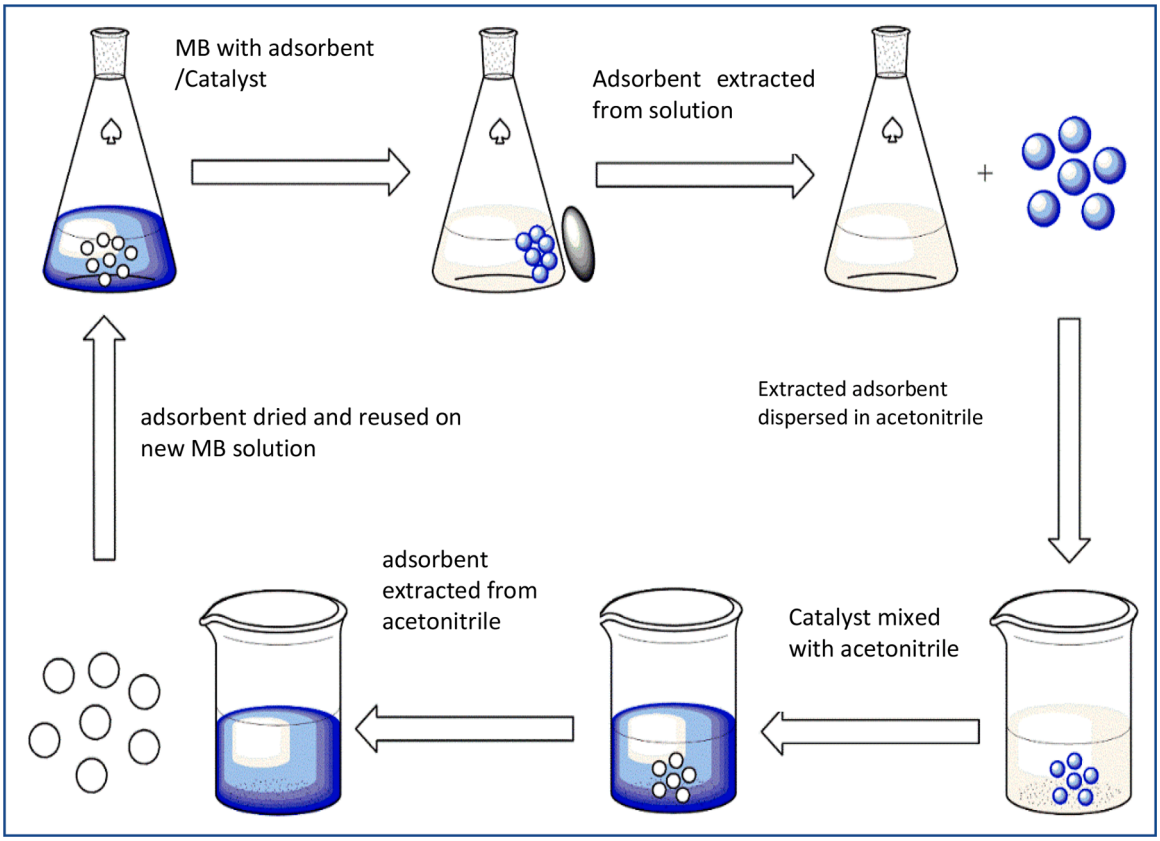

Fig. 15. The recyclability study.

0.00011, and **EJL14** has a K_{obs} value of 0.00027. For the metal loading of 1:50, **EJL6** has a K_{obs} value of 0.00047, **EJL12** has a K_{obs} of 0.00093, and **EJL15** has a K_{obs} value of 0.00006. For the metal loading of 1:100, **EJL7** has a K_{obs} value of 0.00002, **EJL13** has a K_{obs} of 0.00019, and **EJL16** has a K_{obs} value of 0.00033. From Fig. 12, it can be concluded that the effect of $Na_3C_6H_5O_7$ at the metal loading ratio of 1:10 shows that the uncapped catalyst was preferred for MB reduction (**EJL5** vs **EJL11** vs **EJL14**), as it has the highest K_{obs} value. But **EJL5** was unable to retain the reduction of MB as a slight blue colour was observed after 24 hrs of reduction, whilst it was not observed for the phosphine stabilised catalysts, **EJL11** and **EJL14**. For the metal loading ratio 1:50, the PTA stabilised catalysts were preferred for the MB reduction (**EJL6** vs **EJL12** vs **EJL15**), as it has the highest K_{obs} values. For the metal loading ratio 1:100, the PPh_3 stabilised catalyst was preferred for the MB reduction (**EJL7** vs **EJL13** vs **EJL16**).

4.4. The mechanism for MB reduction

From the literature, it is proposed that metal nanoparticles act as electron transfer systems, facilitating the transfer of an electron from $NaBH_4$ to the MB dye. The transfer can be unfavourable due to a large potential difference between the reagents. Hence, metal nanoparticles with an intermediate potential assist can in the transfer of the electron. [20] Au helps in the electron relay from BH_4- (donor) to MB (acceptor). BH_4- ions are nucleophilic, while MB is electrophilic in nature with respect to gold-coated SPIONs. [21] A complete reduction was carried out with all our catalysts at different constant rates as per the discussion with the kinetic studies shown in section 2.5. The observation suggests that the electrons are transferred from $NaBH_4$ to the surface of the catalyst in the initial reaction, with the excess electrons remaining on the catalyst surface and then reducing the MB dye in the second step reaction. This confirms that the catalysts used as AuNPs of different metal loading ratios, with different reducing agents and different ligand stabilisers follow the proposed mechanisms, as shown in Fig. 13.

5. Preliminary MB removal and recycling studies

From the MB dye reduction studies, we separated 50% of the reduced MB solutions into two separate pill vials, one containing the catalyst and the other without catalyst (which we removed after the reaction). It was observed that both solutions–with and without the catalyst–remained clear over an extended period. This led to the investigation of possible MB dye removal from solution by the magnetic catalyst. Therefore, we preliminarily investigated the possible removal of the MB dye and propose that the MB behaves as a stabiliser on our nanoparticle surface, which allowed for the removal of the MB dye from the solution via magnetic extraction. The preliminary results using UV-Vis spectroscopy is presented below. The removal studies were carried out using naked SPIONs, unstabilised gold-coated SPIONs, PTA stabilised gold-coated SPIONs and PPh_3 stabilised gold-coated SPIONs. All the adsorbents were tested with and without thereducing agent, $NaBH_4$.

5.1. Removal of MB in the presence of the reducing agent ($NaBH_4$)

For this investigation, six catalysts/adsorbents (**EJL1, EJL3, EJL6, EJL9, EJL12** and **EJL15**) were selected based on their characteristics as discussed in the previous section. From the kinetic studies, it was seen that the gold-coated SPIONs with the naked SPIONs:Au metal loading ratios of 1:50 (**EJL5** and **EJL12**) were found to be more active in the reduction of MB. The method used for this investigation was as follows: a MB solution of 0.04 mM was prepared and placed into a pill vial. A reducing agent ($NaBH_4$ solution) of 0.05 mM was prepared and added to the MB solutions. Then, an appropriate amount of adsorbents (catalyst) were added to the pill vials containing MB and $NaBH_4$ as shown in Table 6. The reaction mixture in a pill vial were left to react for 24 hrs. The adsorbents were then removed from the reaction mixture using a

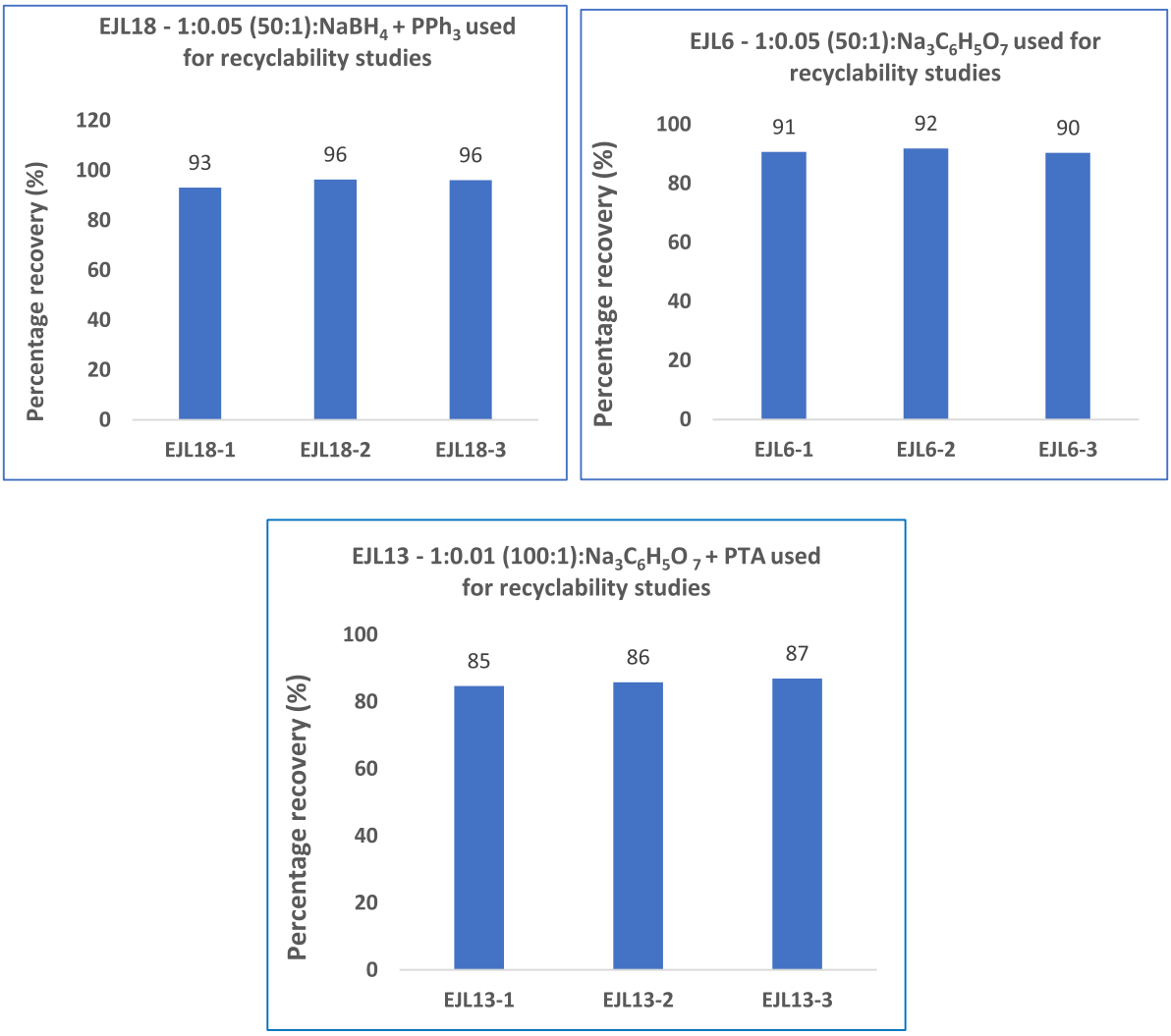

Fig. 16. The percentage recyclability study used for degradation efficiency.

magnet and a clear solution was left in the pill vial (Figure S10, ESI). The MB solutions were analysed before and after the addition of the reducing agent ($NaBH_4$) and the adsorbents.

All the adsorbents prepared using $NaBH_4$ as a reducing agent (**EJL3** and **EJL9**) were the fastest to remove the MB dye, compared to the sodium citrate analogues (**EJL6, EJL12** and **EJL15**). As expected, the naked SPIONs was the least likely to remove the dye, although it is not as slow as the sample without any catalyst. After 24 h, the catalysts were extracted from the MB solutions using a magnet, and the solutions were analysed using the UV–Vis spectrophotometer. The results were presented as seen in Fig. 14. It can be clearly seen that all the catalysts removed the MB dye from the aqueous solution, as the absorbence peak at $\lambda = 666$ nm is absent, showing no presence of MB dye in the aqueous solution.

5.2. Removal of MB without reducing agent ($NaBH_4$)

A similar experiment was done as discussed in Section 5, but this time without the $NaBH_4$ as reducing agent. The adsorbents that were used for this investigation were (**EJL1, EJL2, EJL5, EJL8 EJL11, EJL14** and **EJL17**) and the amount of each adsorbent is shown Table 6. Seven adsorbents were selected for this investigation, unstabilised gold-coated SPIONs, stabilised gold-coated SPIONs and the naked SPIONs to compare their adsorption capabilities in the removal of MB dye from aqueous solution. This time the focus was only at the absorbence values observed at $\lambda = 666$ nm, and from Fig. 14 it was seen that the adsorbents seem reduce the MB dye from solution even without the use of the reducing agent ($NaBH_4$). We postulate that the sulfur moiety on the methylene blue dye structure, coordinates to the Au atom on the surface of the nano-adsorbent. This also explains how the adsorbent removes the dye from the aqueous solution, as there are several Au atoms on the surface of the nano-absorbent, available for the dye to coordinate to via the S-moiety, forming an Au-S bond. The dye is then easily removed along with the adsorbent, via the use of an external magnetic field. Eqn. (10), Table 7, Fig. 7

5.3. Recyclability studies

The adsorbent (catalyst) selected for the recyclability study was **EJL12**. The recyclability of **EJL12** was performed five times using fresh MB dye aqueous solution for each cycle. Fig. 15 summarises all the steps that were carried out to perform the recycling experiment. The catalyst, in the absence of reducing agent, showed the successful removal of the MB dye from solution. Subsequent recycles of the catalyst was also successful with negligible loss of activity between cycles, as shown in Fig. 16. It is proposed that the MB coordinates to the nanoparticle surface, which is then magnetically extracted along with the catalyst from the solution. To recycle the adsorbent, the MB is cleaved from the nanoparticle surface by the addition of acetonitrile, which substitutes the MB on the surface, resulting in an acetonitrile stabilised nanoparticle

and free MB in the acetonitrile solution. The nanoparticles were dried and subsequently reused up to five times, showing similar results throughout. The acetonitrile can be filtered and reused. The UV–Vis spectra of acetonitrile before and after contact with the catalyst (**EJL12**) used for the removal of MB are shown in Figure S11 and Figure S12, (ESI). The spectra clearly showed the transfer of the MB from the adsorbents to the acetonitrile.

The removal percentages achieved with the following adsorbents: **EJL6, EJL13** and **EJL18**, were calculated using Eq. (11): [18]

$$\%Removal = \frac{Ci - Cf}{Ci} \times 100\% \quad (11)$$

where C_i is the MB concentration at $\lambda = 666$ nm and C_f is the MB + catalyst concentration at $\lambda = 666$ nm. The results as seen on the histograms shows that the catalysts used (**EJL6, EJL13** and **EJL18**) could be recovered and removed the MB from three cyclability studies as follows, **EJL6** was up to 91% MB removal, **EJL13** was up to 86% MB removal and **EJL18** was up to 95% MB removal. For the three cycles, the removal efficiencies were almost similar with negligible differences indicating that the adsorbents retained their structural properties during adsorption. These results also concludes that there is not much leaching of gold during the adsorption as each cycle showed similar percentage recoveries.

6. Conclusion

In this paper, we report on the design of 18 novel magnetic nanomaterials, capable of not only reducing the toxic methylene blue dye found in textile wastewater, but also completely removing the dye from the wastewater solution. Gold nanoparticles were immobilised on magnetic supports, and was subsequently stabilised with one of two phosphine ligands, PTA or PPh_3. These nanosystems were fully characterised and gave reproducible results every with a NPs diameter of between 16 and 27 nm, depending on the reducing agent and stabilising ligand employed. 1,3,5-Triaza-7-phosphaadamantane (PTA) were found to be better a better stabiliser than the triphenylphosphine (PPh_3) ligand, as it gave more monodisperse nanoparticles. Upon evaluation of these nanomaterials as catalysts for methylene blue reduction, it was found that these nanosystems were quite active for this reaction, and even upon removal of the catalyst, the solution stayed colourless for a period of 6 months. It's important to note that the unmodified magnetite was very active for this reaction, however, it easily oxidised back to methylene blue, whereas the phosphine modified nanosystem reductions, remained colourless. It could be concluded that using sodium citrate as a reducing agent works better than sodium borohydride on both ligand stabilisers. Upon further investigation, it was found that the MB dye adsorbs onto the surface of the modified nanoparticles, and subsequently gets removed along with the catalyst when an external magnetic field is applied. This was proven via FTIR and UV–Vis monitoring. The MB dye could be desorbed from the nano surface, by simple shaking of the nano-adsorbent in acetonitrile for 30 mins. The nano-adsorbent could subsequently be reused up to 5 times, without any loss in activity. Dye removal without using any reducing agent was also attempted, and it was found that the dye is still removed by the nanomaterials, albeit a little slower than when the $NaBH_4$ is used as a reducing agent. In conclusion, this work entails very exciting results, with an economical and reusable magnetic adsorbent for wastewater treatment, without the use of harmful reducing agents such as $NaBH_4$. Moreover, the removal percentage were consistent in all four cycles.

Declaration of Competing Interest

On behalf of all authors, the corresponding author states that there is no conflict of interest.

Acknowledgements

The financial assistance of the National Research Foundation (NRF) towards this research is hereby acknowledged. Opinions expressed, and conclusions arrived at, are those of the author and are not necessarily to be attributed to the NRF.

Supplementary materials

Supplementary material associated with this article can be found, in the online version, at doi:10.1016/j.surfin.2022.101970.

References

[1] R.G. Saratale, G.D. Saratale, J.S. Chang, S.P. Govindwar, Bacterial decolorization and degradation of azo dyes: a review, J. Taiwan Inst. Chem. Eng. 42 (1) (2011) 138–157.
[2] P. Saikia, A.T. Miah, P.P. Das, Highly efficient catalytic reductive degradation of various organic dyes by Au/CeO_2-TiO_2 nano-hybrid, J. Chem. Sci. 129 (1) (2017) 81–93.
[3] N.T. Nandhini, S. Rajeshkumar, S. Mythili, The possible mechanism of eco-friendly synthesized nanoparticles on hazardous dyes degradation, Biocatal. Agric. Biotechnol. 19 (April) (2019), 101138.
[4] G. Mezohegyi, F.P. van der Zee, J. Font, A. Fortuny, A. Fabregat, Towards advanced aqueous dye removal processes: a short review on the versatile role of activated carbon, J. Environ. Manage. 102 (2012) 148–164.
[5] M. Ghaedi, et al., Removal of methylene blue by silver nanoparticles loaded on activated carbon by an ultrasound-assisted device: optimization by experimental design methodology, Res. Chem. Intermed. 44 (5) (2018) 2929–2950.
[6] S. Raina, A. Roy, N. Bharadvaja, Degradation of dyes using biologically synthesized silver and copper nanoparticles, Environ. Nanotechnol. Monit. Manag. 13 (November 2019) (2020), 100278.
[7] Y. Zhu, et al., Magnetic nanocomposites: a new perspective in catalysis, ChemCatChem 2 (4) (2010) 365–374.
[8] M.B. Gawande, P.S. Branco, R.S. Varma, Nano-magnetite (Fe_3O_4) as a support for recyclable catalysts in the development of sustainable methodologies, Chem. Soc. Rev. 42 (8) (2013) 3371–3393.
[9] H. Maleki, A. Simchi, M. Imani, B.F.O. Costa, Size-controlled synthesis of superparamagnetic iron oxide nanoparticles and their surface coating by gold for biomedical applications, J. Magn. Magn. Mater. 324 (23) (2012) 3997–4005.
[10] Y.C. Chang, D.H. Chen, Catalytic reduction of 4-nitrophenol by magnetically recoverable Au nanocatalyst, J. Hazard. Mater. 165 (1–3) (2009) 664–669.
[11] T. Robinson, G. McMullan, R. Marchant, P. Nigam, Remediation of dyes in textile effluent: a critical review on current treatment technologies with a proposed alternative, Bioresour. Technol. 77 (3) (2001) 247–255.
[12] M. Wierucka, M. Biziuk, Application of magnetic nanoparticles for magnetic solid-phase extraction in preparing biological, environmental and food samples, TrAC - Trends Anal. Chem. 59 (2014) 50–58.
[13] R. Massart, Preparation of aqueous magnetic liquids in alkaline and acidic media, IEEE Trans. Magn. 17 (2) (Mar. 1981) 1247–1248.
[14] J.T. Khutlane, K.R. Koch, R. Malgas-Enus, Competitive removal of PGMs from aqueous solutions via dendrimer modified magnetic nanoparticles, SN Appl. Sci. 2 (6) (2020).
[15] I.O. Wulandari, D.J.D.H. Santjojo, R.A. Shobirin, A. Sabarudin, Characteristics and magnetic properties of chitosan-coated Fe_3O_4 nanoparticles prepared by ex-situ co-precipitation method, Rasayan J. Chem. 10 (4) (2017) 1348–1358.
[16] Z. Ur Rahman, Y.L. Dong, C. Ren, Z.Y. Zhang, X. Chen, Protein adsorption on citrate modified magnetic nanoparticles, J. Nanosci. Nanotechnol. 12 (3) (2012) 2598–2606.
[17] J.L. Lyon et al., "Synthesis of Fe oxide core /Au shell nanoparticles by iterative hydroxylamine seeding," no. Ii, 2004.
[18] O. AA, Kinetic study of decolorization of methylene blue with sodium sulphite in aqueous media: influence of transition metal ions, J. Phys. Chem. Biophys. 2 (2) (2014) 1–7.
[19] M. Nemanashi, R. Meijboom, Synthesis and characterization of Cu, Ag and Au dendrimer-encapsulated nanoparticles and their application in the reduction of 4-nitrophenol to 4-aminophenol, J. Colloid Interface Sci. 389 (1) (2013) 260–267.
[20] N. Gupta, H.P. Singh, R.K. Sharma, Metal nanoparticles with high catalytic activity in degradation of methyl orange: an electron relay effect, J. Mol. Catal. A Chem. 335 (1–2) (2011) 248–252.
[21] A. Blanckenberg, R. Malgas-Enus, Raspberry-like gold-decorated silica (SSx–AMPS–Au) nanoparticles for the reductive discoloration of dyes, SN Appl. Sci. 1 (7) (2019) 1–13.